Comparison of SMOS and SMAP soil moisture retrieval approaches using tower-based radiometer data over a vineyard field

Maciej Miernecki[a], Jean-Pierre Wigneron[b], Ernesto Lopez-Baeza[c],Yann Kerr[d], Richard De Jeu[e], Gabrielle J. M. De Lannoy[f], Tom J. Jackson[g], Peggy E. O'Neill[f], Mike Schwank[h,i], Roberto Fernandez Moran[c], Simone Bircher[d], Heather Laurence[j], Arnaud Mialon[d], Ahmad Al Bitar[d], Philippe Richaume[d]

[a] University of Hamburg, Center for Marine and Atmospheric Sciences (ZMAW), Hamburg, Germany

[b] INRA, Bordeaux Sciences Agro, UMR 1391 ISPA, F-33140 Villenave d'Ornon, France

[c] Faculty of Physics, University of Valencia, 50. Burjassot. 46100 Valencia, Spain

[d] Centre d'Etudes Spatiales de la BIOsphère (CESBIO –– CNES, CNRS, IRD, Université Toulouse III), Toulouse, France

[e] Department of Earth Sciences, VU University Amsterdam, the Netherlands.

[f] NASA GSFC, Greenbelt, MD 20771, USA

[g] USDA-ARS Hydrology and Remote Sensing Laboratory, Beltsville, MD 20705-2350 USA

[h] Gamma Remote Sensing, Worbstr. 225, CH-3073 Gümligen, Switzerland

[i] Swiss Federal Research Institute WSL, Zürcherstrasse 111, 8903 Birmensdorf, Switzerland

[j] European Centre for Medium-Range Weather Forecasts (ECMWF), Reading, UK

ABSTRACT

The objective of this study was to compare several approaches to soil moisture (SM) retrieval using L-band microwave radiometry. The comparison was based on a brightness temperature (T_B) data set acquired since 2010 by the L-band radiometer ELBARA-II over a vineyard field at the Valencia Anchor Station (VAS) site. ELBARA-II, provided by the European Space Agency (ESA) within the scientific program of the SMOS (Soil Moisture and Ocean Salinity) mission, measures multiangular T_B data at horizontal and vertical polarization for a range of incidence angles (30°-60°). Based on a three year data set (2010-2012), several SM retrieval approaches developed for spaceborne missions including AMSR-E (Advanced Microwave Scanning Radiometer for EOS), SMAP (Soil Moisture Active Passive) and SMOS were compared. The approaches include: the Single Channel Algorithm (SCA) for horizontal (SCA-H) and vertical (SCA-V) polarizations, the Dual Channel Algorithm (DCA), the Land

Parameter Retrieval Model (LPRM) and two simplified approaches based on statistical regressions (referred to as 'Mattar' and 'Saleh'). Time series of vegetation indices required for three of the algorithms (SCA-H, SCA-V and 'Mattar') were obtained from MODIS observations. The SM retrievals were evaluated against reference SM values estimated from a multiangular 2-Parameter inversion approach. The results obtained with the current base line algorithms developed for SMAP (SCA-H and -V) are in very good agreement with the 'reference' SM data set derived from the multi-angular observations ($R^2 \approx 0.90$, RMSE varying between 0.035 and 0.056 m^3/m^3 for several retrieval configurations). This result showed that, provided the relationship between vegetation optical depth and a remotely-sensed vegetation index can be calibrated, the SCA algorithms can provide results very close to those obtained from multi-angular observations in this study area. The approaches based on statistical regressions provided similar results and the best accuracy was obtained with the 'Saleh' methods based on either bi-angular or bipolarization observations ($R^2 \approx 0.93$, RMSE ≈ 0.035 m^3/m^3). The LPRM and DCA algorithms were found to be slightly less successful in retrieving the 'reference' SM time series ($R^2 \approx 0.75$, RMSE ≈ 0.055 m^3/m^3). However, the two above approaches have the great advantage of not requiring any model calibrations previous to the SM retrievals.

1. Introduction

Surface soil moisture plays a major role in the water and energy budgets of continental surfaces, which has direct implications for hydrological, climate, and weather forecasting models. L-band passive microwave remote sensing is one of the most promising approaches to monitor this variable at the global scale with frequent revisiting times (Jackson et al., 1995; Kerr et al., 2001, Njoku et al., 2003; De Lannoy et al., 2013). Three recent or planned space missions use this technology: SMOS (launched end of 2009), Aquarius (launched in June of 2011) and SMAP (launch scheduled in November 2014).

The Soil Moisture and Ocean Salinity (SMOS) mission is the first spaceborne mission dedicated to soil moisture (SM) mapping. SMOS has multi-angular capabilities which are exploited by the SM retrieval approach: SM and vegetation optical depth τ (used to parameterize vegetation attenuation and emission) are retrieved simultaneously based on SMOS multi-configuration observations, in terms of polarizations and incidence angles. Aquarius is a combined passive/active L-band microwave instrument which consists of a set

of three radiometers and a scatterometer, operating at 1.4 GHz and 1.26 GHz respectively (Levine et al., 2010). The primary mission objective of Aquarius is to provide global observations of surface sea salinity once every 7 days. However, Aquarius has also potential capabilities to monitor soil moisture at global scales (Luo et al., 2013, Bindlish et al., 2013). SMAP incorporates a radar and a radiometer, both operating at L-band and at the incidence (observation) angle $\theta = 40°$. The spatial resolutions of the corresponding active- and passive microwave signatures are ~ 39 km x 47 km and ~ 1 km x 1 km, respectively. The mission concept is to combine the complementary attributes of the radar observations (high spatial resolution but lower soil moisture accuracy) and radiometer observations (higher soil moisture accuracy but coarse spatial resolution) to retrieve SM at a spatial resolution of 9 km, and the freeze-thaw state at a spatial resolution of 3 km (Entekhabi et al., 2010; O'Neill et al., 2013).

Several SM retrieval approaches have been developed in the context of these L-band space missions. As noted above, in the operational SMOS SM retrieval algorithm, SM and vegetation optical depth at nadir (τ_{NAD}) are retrieved simultaneously based on SMOS multiangular and bipolarization observations (Wigneron et al., 1995, 2000; Kerr et al., 2012). The 2-Parameter (2-P) retrievals of SM and τ_{NAD} are obtained from inversion of the L-MEB (L-band Microwave Emission of the Biosphere) model (Wigneron et al., 2007). This forward model is based on the so-called τ-ω model (Mo et al., 1982) and it includes a number of parameterizations to capture effects of vegetation structure and soil roughness on polarization and angular properties of L-band T_B emitted from land surfaces. The inversion of L-MEB considering SM and τ_{NAD} as the requested parameters (referred to as 'L-MEB 2-P' inversion) is implemented in the operational algorithms used to compute the Level 2 (distributed by ESA) and Level 3 (distributed by the Centre Aval de Traitement des Données SMOS (CATDS), Berthon et al., 2012) SMOS products. In parallel to this operational retrieval method, several simplified methods have been developed to exploit the capability of L-band radiometers to provide information on land surface states such as SM. For instance, Wigneron et al. (2004) and Saleh et al. (2006) have evaluated statistical regressions based on bi-polarization or bi-angular T_B data. Mattar et al. (2012) have evaluated similar regression methods that also use a vegetation index estimated from ancillary remotely sensed observations (such as the Normalized Difference Vegetation Index (NDVI) or the Leaf Area Index (LAI)) to account for vegetation effects. Moreover, methods based on Neural Networks have been and are currently evaluated (Liu et al., 2002; Rodriguez et al., 2003).

97 The general retrieval approach proposed for SMAP is different from the operational SMOS
98 SM retrieval: SMAP observations will be available for the sole incidence angle of 40°, but
99 make use of the complementary information provided by the active- (radar) and the passive
100 (radiometer) L-band data. In the initial release of the ATBD (Algorithm Theoretical Basis
101 Document) written for the retrievals from SMAP's radiometer (O'Neill et al., 2013), four soil
102 moisture retrieval algorithms are suggested for evaluation during the pre- and post-launch
103 calibration and validation activities: (i) the single-channel algorithm at H polarization (SCA-
104 H) which is the current SMAP baseline algorithm, (ii) the single-channel algorithm at V
105 polarization (SCA-V), (iii) the dual-channel algorithm (DCA), and (iv) the Land parameter
106 retrieval model (LPRM). In the SCA-H and –V algorithms, vegetation is accounted for by the
107 τ-ω model as in L-MEB. However, optical depth at nadir (τ_{NAD}) is not retrieved as for SMOS.
108 Instead it is estimated from the linear relation $\tau_{NAD} = b \cdot VWC$ between τ_{NAD} and vegetation
109 water content (VWC) (Jackson et al. (1991)). Thereby, values of the b-parameter are assumed
110 polarization independent and will be provided from a land cover look up table, and the VWC
111 is estimated from values of the NDVI Index. The DCA retrieval approach is very similar to
112 the one used for SMOS. The only difference is that the inversion is based on the minimization
113 of a cost function accounting for the Root Mean Square Error (RMSE) between measured and
114 simulated bi-polarized T_B observations at one incidence angle, whereas multi-angular
115 observations are used for SMOS. In the LPRM algorithm, the Microwave Polarization
116 Difference Index (MPDI) and the observed emissivities are used to derive the vegetation
117 optical depth τ (Meesters et al., 2005). In a second step, SM is retrieved with an optimization
118 routine that minimizes the error between the modelled and observed H-polarized brightness
119 temperatures (Owe et al., 2008; De Jeu et al., 2009).
120 In this study, these different retrieval algorithms were compared using a 3-year long
121 multiangular T_B data set acquired by the L-band radiometer ELBARA-II over a vineyard field
122 (MELBEX-III) at the Valencia Anchor Station (VAS) site (Schwank et al., 2012, Wigneron et
123 al., 2012). Applications of the retrieval methods can be made at large scales from satellite
124 observations but also at more local scale for long term SM monitoring from ground based
125 instruments mounted on different types of platforms: towers as for ELBARA-II (de Rosnay et
126 al., 2006; Schwank et al., 2012; Schlenz et al., 2012, etc.); trucks (Hornbuckle et al., 2004;
127 Kurum et al., 2009) or from the top of a mountain as in Pellarin et al. (2013).
128 ELBARA-II (Schwank et al. 2010), developed by GAMMA Remote Sensing AG
129 (Switzerland) and funded by the ESA, provides T_B at horizontal and vertical polarization for a

range of observation angles (30°-60°). The ELBARA-II T_B observations were acquired since 2010 and a 3-year T_B data set is available for the MELBEX-III site. As an accurate estimation of SM from ground based measurements over the MELBEX-III site could not be achieved because of very frequent agricultural practices within the field, it was considered that representative SM values (referred to as 'reference' SM data set) over the ELBARA-II footprints were obtained from multi-angular 2-P L-MEB retrievals. Moreover, the 2-P L-MEB approach also provided retrievals of optical depth at nadir (τ_{NAD}). These latter values were used to calibrate the relationships between τ_{NAD} and NDVI, which are required in the SCA-H and SCA-V algorithms. Based on these 'reference' SM and τ_{NAD} data sets and the ELBARA-II T_B observations, seven SM retrieval approaches were evaluated and compared: the four methods considered presently in the SMAP ATBD based on bi-polarization observations at one observation angle ($\theta = 40°$ for SMAP) and three regression methods (Saleh et al, 2006 and Mattar et al., 2012) developed in the framework of SMOS research activities and based on bi-angular or bipolarization observations. The results of this evaluation are discussed in the context of the improvement and development of the SM retrieval algorithms.

2. Materials and method

2.1. The ELABARA-II radiometer at MELBEX-III (VAS site)

The study was based on T_B measurements made by the ELBARA-II radiometer over the 2010-2012 period within the VAS site. ELBARA-II was installed in September 2009 at the MELBEX-III vineyard field (referred to as M-III), close to Caudete de las Fuentes, on the Utiel-Requena Plateau at ~ 800 m a.s.l., in the region of Valencia, Spain (39°31'18.18"N, 1°17'29.64"W). This site is one of the reference sites selected by ESA in Europe within the SMOS science program.

All details concerning the ELBARA-II instrument and the M-III experiment set up are given in Schwank et al. (2010, 2012), and Wigneron et al. (2012). Only a brief summary of the main information concerning this experiment is presented here.

The ELBARA-II radiometer was set up 17 meters above ground to monitor a vineyard that is representative of the main land use of the VAS region. The ELBARA-II was equipped with an elevation tracker that allows measurements at specific observation angles θ varying

between $30° \leq \theta \leq 330°$ with $\theta = 180°$ being the zenith direction. Every 30 minutes, automated "elevation scans" are carried out that provide T_B at horizontal and vertical polarizations at observation angles between $\theta = 30°$ and 70° with steps of 5°. Between each elevation scan, measurements are made at the $\theta = 45°$ every 10 minutes. Once a day, at 23:55 local time, the radiometer is automatically positioned at 150º to carry out sky calibration measurements. The absolute accuracy of the ELBARA-II measurements was estimated to be better than ±1 K over the course of 2010-2012. During short time periods, no measurement could be acquired over the vineyard field due to experiments using reflecting foils (Schwank et al., 2012) or due to technical issues: in 2010 (DoY 222 - DoY 245, DoY 312 - DoY 337) and in 2011 (DoY 41 – DoY 62; DoY 84 – DoY 133). The ELBARA-II observations were slightly affected by Radio Frequency Interferences (RFI) caused by active microwave systems violating the protected part of the L-Band (1400 MHz – 1427 MHz). Efforts made by the Spanish administrative authorities in 2010 to mitigate RFI disturbances resulted in a significant decrease since the beginning of July in 2010 (~ DoY 190). Most RFI events result in steep increases in the time variations of the measured T_B (larger than 30K at minimum) and unrealistic T_B values (larger than 330 K). These RFI events were detected manually from the ELBARA-II T_B data set. To be consistent with the overpass times of SMOS and SMAP, only T_B measurements made at 6 am and 6 pm local time are considered in this study.

2.2. *In situ* measurements

Concurrent with the ELBARA-II observations, ground measurements were obtained within the M-III vineyard. Soil profiles of the volumetric soil moisture [$m^3 \cdot m^{-3}$] and temperature were acquired up to about 1 m (Wigneron et al., 2012). Vineyard cultivation practices are carried out frequently within the field (for weeding and pest control, winter and summer pruning, cluster thinning, etc.) so that SM probes could not be installed permanently within the ELBARA-II footprints. Only two Delta-T Theta Probes measuring the volumetric SM of the top 0-6cm soil layer were installed at the border of the field where no field work was carried out. It is our opinion that these SM probes cannot provide SM values representative of the field conditions as seen by the ELBARA-II instrument and have not been used in the analysis presented here (Wigneron et al., 2012).

A meteorological station located at the VAS (coordinates: 39º34'15''N, 1º17'18''W, 813 m a.s.l.), a few kilometres from the M-III site provided the standard meteorological variables (air temperature, wind speed, air humidity, etc.). Over the VAS site, the average value of the total yearly precipitation over the ten years prior to 2010 is P = 461 mm. For the three years considered in this study; 2010 was wet (P = 538.2 mm) and was followed by a 'dry' and a 'very dry' year in 2011 and 2012 (P = 379.2 mm in 2011 and P = 288.6 mm in 2012).

Details concerning the soil and vegetation conditions at the M-III site are provided in Wigneron et al. (2012). The field-site observed with ELBARA-II is typical of vineyards in the VAS region (the spacing between each plant is ~ 2 m and that between each row is ~ 3 m). Two field experiments in 2007 and 2010 led to similar values of the maximum Leaf Area Index, $LAI_{MAX} \approx 2.2$. To monitor the time variations in the vegetation characteristics over the growing season, we used the NDVI index from the MODIS products (16 day NDVI composite of 250 m MODIS data; MODIS (2010)). As the field was large enough (larger than 300 m x 300 m), it can considered that the MODIS NDVI time variations are representative of the vegetation conditions as seen by the ELBARA-II radiometer operated at the M-III site.

In order to monitor the evolution of the surface roughness over time, field measurements were made by means of measuring mechanically two-dimensional profiles of the ground surface. For this purpose, a 2 m needle board with 201 needles, movable in the vertical direction and with 1 cm spacing between needles was used (Mialon et al. (2012)). The needle board was leveled and placed on the ground such that the needles were allowed to fall until they touched the soil surface. Subsequently, photos of the profile created by the needle heights were taken and digitized to compute soil roughness parameters. On each of the seven days during 2012 when roughness measurements were performed, approximately 8 to 12 profiles were taken within the ELBARA-II footprints. Different locations and orientations (perpendicular and parallel to the vegetation rows) were considered in computing representative information on the standard deviation of soil surface height (S_D, cm), and correlation length (L_C, cm). Time variations in the average values of S_D and L_C are shown in Fig. 1 for the seven days of measurements in 2012. The corresponding annual mean values are $\langle S_D \rangle$ = 2.2 cm, $\langle L_C \rangle$ = 6.2 cm.

2.3 L-MEB modelling and inversion

The data set considered as a reference in this study was obtained using the 2-P L-MEB inversion approach to obtain retrievals of SM and τ_{NAD} (Wigneron et al., 2000). There are many reasons to use this retrieved data set as a reference.

First, the SM data set retrieved from tower-based remote sensing observations can be considered as representative of the SM conditions over the whole ELBARA-II footprint (this is usually a complex task using field probes distributed within the field). Second, the 2-P L-MEB method, based on multi-angular observations, has been validated in many studies against experimental data sets for a variety of soil and vegetation conditions (Wigneron et al., 1995, 2007; Pardé et al., 2003, 2004, Saleh et al., 2006; Panciera et al., 2009; Cano et al., 2010; Schlenz et al., 2012, etc.), and its accuracy and robustness has been evaluated theoretically (Wigneron et al., 2000). The 2-P L-MEB method is currently implemented in the official SMOS retrieval algorithm (Kerr et al, 2012). Third, the 2-P L-MEB approach has the advantage of providing retrievals of optical depth at nadir (τ_{NAD}). These latter values were used to calibrate the relationships between τ_{NAD} and NDVI, which are required in the SCA-H and SCA-V algorithms. Moreover, it can not be considered that one method can benefit from the use of 2-P L-MEB retrieval method as a reference: the equations of the L-MEB model, used in the 2-P L-MEB approach, are also the basis of the SCA-H, SCA-V, DCA and LPRM algorithms.

A detailed description of the L-MEB model is given in Wigneron et al. (2007) and a brief summary of the main L-MEB equations and of additional parameterizations developed since 2007 is given in the following. The L-MEB model is based on a zero-order solution of the radiative transfer equations: the so called τ-ω model, where the optical depth τ accounts for extinction effects within the canopy and the effective scattering albedo ω (-) accounts for scattering effects (Mo et al., 1982; Kurum et al., 2013). To incorporate the SMOS multi-angular feasibility, several additional parameterizations are used in L-MEB to account for effects of the vegetation structure and soil roughness on L-band brightness temperatures emitted from vegetated land surfaces.

In local thermal equilibrium the emissivity e_{GP} of the ground at horizontal (p = H) and vertical (p = V) polarization is related to the corresponding reflectivity r_{GP} of the soil (the ground) observed at the angle θ:

$$e_{GP}(\theta) = 1 - r_{GP}(\theta) \quad (1)$$

253 The soil reflectivity r_{GP} can be expressed as the reflectivity r^*_{GP} of a specular surface and the
254 roughness model parameters Q_R, H_R and N_{RP} as:

255 $$r_{GP}(\theta) = [(1-Q_R)\, r^*_{GP}(\theta) + Q_R\, r^*_{GQ}(\theta)] \exp(-H_R \cos^{NRP}(\theta)) \quad (2)$$

256 In this equation, H_R parameterizes the intensity of the roughness effects, Q_R parameterizes the
257 polarization mixing effects, and N_{RP} is used to account for the specific effects of roughness on
258 the trend of soil reflectivity r_{GP} as a function of incidence angle and polarization. The
259 reflectivity of a specular surface r^*_{GP} was computed using the Fresnel equations as a function
260 of θ and of the effective soil dielectric permittivity ε_G. The latter was computed from soil
261 moisture SM, soil effective temperature T_G, and from the clay fraction using the dielectric
262 mixing model of Mironov et al. (2012), referred to as the 'Mironov' model in the following.
263 This is in contrast to the earlier study Wigneron et al. (2007), where the Dobson model
264 (Dobson et al., 1985) was used to estimate ε_G.

265 We used the recent results of Lawrence et al. (2013) to estimate the values of the roughness
266 model parameters (Q_R, H_R and N_{RP}). These parameters were assumed as constants in time,
267 and therefore computed from the annual average value $\langle S_D \rangle$ of the standard deviation of the
268 soil surface height and the corresponding annual mean $\langle L_C \rangle$ of the correlation length (Fig. 1).
269 To be consistent with the general approach considered for SMAP we assumed that $N_{RV} = N_{RH}$
270 = 0 (O'Neill et al., 2013). On that assumption, the roughness parameters H_R and Q_R were
271 computed as (Lawrence et al., 2013):

272 $$H_R = 1.762\,(1 - \exp(-Z_S/1.85)) \text{ and } Q_R = 0.05\, H_R \quad (3)$$

273 where $Z_S = (S_D)^2 / L_C$ (cm)

274 Considering the annual mean values $\langle S_D \rangle$ = 2.2 cm and $\langle L_C \rangle$ = 6.2 cm measured over the M-III
275 site in 2012, we obtained Z_S = 0.78 cm, H_R = 0.606, Q_R = 0.0303.

276 In this study, we considered a composite soil-vegetation surface temperature T_{GC} for the
277 effective temperature T_G of the ground (the soil) and the vegetation canopy T_C. The composite
278 effective temperature T_{GC} of the ELBARA-II footprints was computed from the ERA-
279 INTERIM 0-7 cm soil temperature product ($T_{E\text{-}07}$). ERA-INTERIM is the latest ECMWF
280 (European Centre for Medium-Range Weather Forecasts) global atmospheric reanalysis of the
281 period 1979 to the present (Dee et al., 2011) with a temporal resolution of 3 hours and a

spatial resolution of 0.75° (corresponding to about 100 km resolution over the VAS site). The accuracy of this estimate was considered to be sufficient in several studies investigating SM retrievals from L-band observations (Pardé et al., 2004; Wigneron et al., 2012).

As noted above, we used the τ - ω model to compute the upwelling emission (T_B) from the two layer soil-vegetation medium. T_{BP} (p = H, V) is the sum of three terms: (1) the direct upwelling vegetation emission, (2) the downwelling vegetation emission reflected by the soil and attenuated by the canopy layer, and (3) upwelling soil emission attenuated by the canopy:

$$T_{BP} = (1-\omega_P)\,(1-\gamma_P)\,(1 + \gamma_P\, r_{GP})\,T_C + (1-r_{GP})\,\gamma_P\,T_G \quad (4)$$

where $T_G = T_C = T_{GC} = T_{E\text{-}07}$ is assumed in this study, and r_{GP} is the soil reflectivity computed with (2) and (3). γ_P is the vegetation attenuation factor which is related to the optical depth τ_P as (Beer's law):

$$\gamma_P = \exp(-\tau_P / \cos\theta) \quad (5)$$

To account for vegetation anisotropies, the optical depth $\tau_P(\theta)$ at the observation angle θ is expressed with a parameterization involving the optical depth τ_{NAD} at nadir ($\theta = 0°$) :

$$\tau_P(\theta) = \tau_{NAD}\,(\sin^2(\theta).tt_P + \cos^2(\theta)) \quad (\text{at } p = V, H) \quad (6)$$

The parameters tt_V (-) and tt_H (-) account for the angular dependence of $\tau_P(\theta)$. As found in Wigneron et al. (2012), we considered that $tt_H = 1$ (default L-MEB value) and that the tt_V parameter is free in the retrieval process, to account for the effects of the vine stocks, with a preferential vertical orientation. So in reality, a 3-Parameter retrieval approach is made in this study, but the notation 2-P is kept, as only SM and τ can be considered as variables of interest for applications.

The values of the effective scattering albedo ω_P were found to be close to zero over most of the non-forested vegetation covers (Grant et al., 2008; Kurum et al., 2013). The value of ω_P was set equal here to 0.02 for both polarizations. A summary of the values of the soil and vegetation L-MEB parameters used in this study over the M-III site and described above is given in Table 1.

The 2-P L-MEB inversions were based on bi-polarization and multiangular T_B measurements using a minimization procedure of a cost function evaluating the difference between the L-

MEB simulations and the T_B measurements (Wigneron et al., 2000, 2007, 2012). The retrievals were based on ELBARA-II T_B data acquired with the automated elevation scans (section 2.1) performed for the observation angles θ = 30°, 35°, 40°, 45°, 50° (corresponding roughly to the limit of validity of L-MEB at large incidence angles). As noted above, only T_B measurements made at 6 am and 6 pm will be considered in this study. Especially for the measurements at 6 am temperature gradients across the vegetation and the soil are minimal (Kerr et al., 2001).

2.4 Description of the different SM retrieval methods

As mentioned in the introduction, seven SM retrieval approaches were evaluated and compared in this study: the four methods considered presently in the SMAP ATBD for the passive-only product and three regression methods (described in Saleh et al (2006) and Mattar et al. (2012)) developed in the context of SMOS. The retrieved SM values were compared to a 'reference' SM data set obtained from the 2-P L-MEB inversion, which was assumed to be representative of the SM values over the ELBARA-II footprint. The seven SM retrieval approaches are described in the following sections. As is the case for the 2-P L-MEB method, these seven methods use the τ-ω radiative transfer model (described above) to account for the vegetation effects and they all assume τ_{NAD} is independent of polarization and incidence angle ($\tau_V(0^o) = \tau_H(0^o) = \tau_{NAD}$). They are based on the same equation (1) to model the roughness effects, considering that $N_{RV} = N_{RH} = 0$. Furthermore, as implemented here they all use the 'Mironov' equations to compute the effective soil dielectric permittivity ε_G. All of the parameters listed in Table 1 for the 2-P L-MEB method are accounted for in the seven SM retrieval methods considered. Only a very brief description of the SCA-H, SCA-V, DCA and LPRM methods will be given here as a detailed description of these methods is available in the initial release of the ATBD. All these four methods were applied to the ELBARA-II T_B data at the incidence angle of 40° corresponding to the SMAP observations. A summary of the input variables required for the seven different retrieval methods, as well as for the reference algorithm 2-P L-MEB, is given in Table 2.

2.4.1 Single Channel Algorithms (SCA-H and SCA-V).

The Single Channel Algorithm (SCA-H), based on horizontally polarized T_B observations, is the current SMAP baseline, but the same algorithm can also be applied to vertically polarized T_B data (SCA-V). In SCA-H, brightness temperatures are converted to emissivity using a surrogate for the temperature of the emitting surface layer (in this study, the soil temperature provided by ECMWF (T_{E-07}) is used). The derived emissivity is corrected for vegetation and surface roughness to obtain the soil emissivity. Finally, a dielectric mixing model (the 'Mironov' model in this study) is used to obtain soil moisture SM from the soil dielectric constant ε_G using the Fresnel equations.

In this investigation, SCA-H and SCA-V are based on the same corrections of vegetation (using the τ-ω model), and soil roughness effects (using the H_R and Q_R parameters) as those used for the 2-P L-MEB method.

τ_{NAD} is estimated from the vegetation water content (VWC) as

$$\tau_{NAD} = b \, . \, VWC \qquad (7)$$

where b is a proportionality factor mainly depending on the vegetation structure.

For SMAP, values of b will be provided by means of a land cover look up table and the baseline approach utilizes a set of land cover-based equations to estimate VWC from values of NDVI. The following equation is used for cropland (O'Neill et al, 2013):

$$VWC = (1.9134 \times NDVI^2 - 0.3215 \times NDVI) + Stemfactor \times (NDVI_{ref} - 0.1) / (1 - 0.1) \qquad (8)$$

where Stemfactor parameter is the product of the average height of a land cover class and the ratio of sapwood area to leaf area; $NDVI_{ref}$ is assumed to be equal to the maximum value of NDVI time series (the value of $NDVI_{ref}$ was set equal here to 0.4696 from the analysis of the MODIS NDVI observations over the 2010-2012 period). In this study, the b and Stemfactor parameters were calibrated prior to the inversion process, as described in Section 2.5.

2.4.2 The Dual Channel Algorithm (DCA)

The Dual Channel Algorithm (DCA) is an extension of the SCA and uses both H-polarized and V-polarized T_B observations to simultaneously retrieve SM and VWC (O'Neill et al, 2013). As in the 2-P L-MEB algorithm, the SM and τ_{NAD} variables are adjusted iteratively until the root mean square difference between the simulated and observed T_B is minimized. There are differences between 2-P L-MEB and DCA algorithms. Firstly, T_B data at $\theta = 40°$ are used for DCA, while multiangular data are used for 2-P L-MEB. Secondly, the tt_V

parameter (accounting for an angular dependence of τ) is retrieved in 2-P L-MEB, while DCA does not account for this dependence. Except for the tt_V and tt_H parameters, all vegetation and soil parameters used in DCA are the same as those used in the 2-P L-MEB method (Table 1).

2.4.3 Land Parameter Retrieval Model (LPRM)

The LPRM approach uses an analytical solution for the derivation of the vegetation optical depth. This solution uses the Microwave Polarization Difference Index (MPDI) and the observed surface emissivity (e_H and e_V) as input and is based on the assumption that the values of the vegetation optical depth are the same for both polarization ($\tau_V = \tau_H$). The MPDI index is calculated from the brightness temperature at H- and V polarizations as follows (Meesters et al., 2005):

$$MPDI = (T_{BV} - T_{BH}) / (T_{BV} + T_{BH}) \quad (8)$$

Then based on equation (4) of the τ-ω omega model, soil moisture is retrieved using an optimization routine that minimizes the RMSE between the modelled and observed H-polarized brightness temperatures. As for SMOS, the vegetation optical depth at this optimized soil moisture value is an additional retrieval result. As noted in O'Neill et al. (2013), the LPRM was implemented on multifrequency satellites such as AMSR-E, where also the Ka-band V-polarized channel is used to retrieve physical temperatures of the scene observed. This latter can also be estimated from re-analysis or near real time data from weather prediction centres (Parinussa et al., 2011), as is done in the current SMOS SM retrieval algorithm (Kerr et al., 2012). Only a few studies (e.g. de Jeu et al., 2009) have examined the applicability of this model at L-band frequencies, although the analysis of SMOS data with LPRM is currently underway. All detailed equations of the LPRM approach are given in (Owe et al., 2001; Meesters et al., 2005, Owe et al., 2008, de Jeu et al., 2009, Chung et al., 2013). As for DCA, except for the tt_V and tt_H parameters which are not relevant here, all vegetation and soil parameters used in LPRM are the same as those used in the 2-P L-MEB method (Table 1).

2.4.4 Linear regression methods (Saleh et al., 2006; Mattar et al., 2012)

Two methods based on regression equations developed by Saleh et al. (2006) and Mattar et al. (2012) were evaluated in this study. Both methods were numerically derived from the equations of the τ-ω model assuming, as for LPRM, that the value of the effective scattering albedo is $\omega_P = 0$, and that the values of optical depth τ_P are the same for both polarizations p = H, V. These methods are physically-based. However, as the development of an analytical formulation would be complex, most of the time they are used as regressions methods. As shown by Saleh et al. (2006), a key interest in these regression methods is that they can be used for varying roughness and vegetation conditions over time: no additional information about temporal changes in these two state variables (such as NDVI or LAI for vegetation for instance) is required. These regression methods have been used in several studies based on *in situ*, airborne or spaceborne (SMOS) observations (Albergel et al., 2011; Parrens et al., 2012; Calvet et al., 2011, etc.)

The method of Saleh et al. (2006) can be applied to observations made either at the two incidence angles θ_1 and θ_2 (referred to as 'Saleh' bi-angular):

$$\ln(SM) = a_2 \ln(\Gamma_P(\theta_1)) + a_1 \ln(\Gamma_P(\theta_2)) + a_0 (\theta_1, \theta_2, p) \quad (9)$$

or to bi-polarization observations made at one observation angle θ (referred to as 'Saleh' bi-polarization):

$$\ln(SM) = b_2 \ln(\Gamma_H(\theta)) + b_1 \ln(\Gamma_V(\theta)) + b_0 (\theta) \quad (10)$$

where $\Gamma_P(\theta)$ is the reflectivity of the soil-vegetation system at polarization p (p=V or p=H), defined as

$$\Gamma_P(\theta) = 1 - T_{BP} (\theta) / T_{GC} \quad (11)$$

where the composite soil vegetation surface temperature T_{GC} was estimated from the ERA-INTERIM 0-7cm soil temperature product (T_{E-07}).

The method of Mattar et al. (2012) is very similar and can be written as (referred to as 'Mattar'):

$$\ln (SM) = c_2 \ln (\Gamma_P(\theta)) + c_1 NDVI + c_0 (\theta, p) \quad (12)$$

where the NDVI is considered here as a proxy for optical depth, as in the SCA-H and SCA-V methods.

435 In the above equations (9), (10) and (12), the parameters (a_0, a_1, a_2), (b_0, b_1, b_2) and (c_0, c_1, c_2)
436 are regression coefficients, which are assumed to be constant in time and have to be calibrated
437 over each pixel. In this study, in the 'Saleh bi-polarization' equation (10), we used the
438 observation angle $\theta = 40°$ as used in the other retrieval methods. In the 'Saleh bi-angular'
439 equation (9), we used H-polarized bi-angular observations at $\theta_1 = 30°$ and $\theta_2 = 50°$. In the
440 'Mattar' equation (12), we used H-polarized observations at $\theta = 40°$. These latter
441 configurations were found to be the best for SM retrievals (results not shown here).
442

443 **2.5 Method calibration**

444 In this study, the SCA-V, SCA-H, DCA and LPRM methods were based on the L-MEB
445 model parameters given in Table 1. In addition, some model parameters specific to some
446 methods had to be calibrated. The DCA and LPRM methods did not require any additional
447 calibration. Conversely, in the SCA-V and SCA-H methods, the two parameters b and
448 Stemfactor, used to link NDVI and optical depth, had to be calibrated. Moreover, the three
449 'regression' methods 'Saleh bi-angular', 'Saleh bi-polarization' and 'Mattar' did not require
450 any L-MEB parameters but required the calibration of three coefficients (a_i), (b_i) or (c_i) ($i = 0$,
451 1 and 2) used in equations (8), (9) and (11), respectively.
452 The calibration of the above parameters and coefficients was performed three times, using one
453 year of data for calibration and the two other years for validation. To calibrate the b and
454 Stemfactor parameters in SCA-H and SCA-V, a multilinear regression method was used to fit
455 the optical depth derived from equations (6) and (7) to the 'reference' optical depth τ_{NAD}
456 retrieved from the 2-P L-MEB method. The obtained values for all three calibration years
457 (2010, 2011 and 2012) are given in Table 3.
458 Similarly, to calibrate the three coefficients in the regression equations of the 'Saleh bi-
459 angular', 'Saleh bi-polarization' and 'Mattar' methods, a multilinear regression method was
460 used to minimize the difference between the retrieved SM derived from equations (9), (10) or
461 (12) to the 'reference' SM values retrieved from the 2-P L-MEB method. The obtained values
462 of the coefficients for all three methods and all three calibration years (2010, 2011 and 2012)
463 are given in Table 3.
464
465

466 **3. Results**

3.1. Reference values of SM and τ_{NAD}

As outlined above, the 'reference' values of soil moisture (SM) and optical depth at nadir (τ_{NAD}) were retrieved from the multiangular T_B data measured by the ELBARA-II instrument. The T_B measured $\theta = 40°$ for the time period 2010-2012 are shown in Fig. 2. A clear seasonal cycle in the T_B time-series can be seen, with maximum values of T_B during summer and lower T_B values during winter. This annual cycle is related to the vegetation growth cycle, beginning in April and ending in November, and to the soil moisture conditions, which are generally drier during the summer period.

However, as already noted in Section 2.2, significantly wetter/drier conditions were encountered in 2010/2012, respectively, which is reflected in the observed T_B trends over the MELBEX-II site with lower values during summer 2010 compared to summer 2012. Based on these T_B observations, the retrieved values of SM and τ_{NAD} were computed from the 2-P L-MEB method and they are illustrated in Fig. 3a-b. As discussed in Jackson et al. (2012), conditions of standing water during or shortly after intensive rainfalls should be flagged. In this study, to avoid these conditions, all retrieved values of SM which were found to be larger than the saturation value SM_{SAT} were not considered (SM_{SAT} was set equal to 0.5 m^3/m^3 over the M-III site as computed by Juglea et al. (2010)). Note that due to this data filtering, the number of SM data used in the comparison may vary slightly from one approach to the other.

In accordance with the above-discussed T_B trends one can see that rainy conditions led generally to higher values of SM throughout the year in 2010 and during the winter period in 2011 and 2012 (Fig. 3a). Drier conditions during the second half of 2011 and 2012 led to rather long time intervals of lower SM values.

The vegetation cycle could be clearly distinguished from the time variations in both the optical depth at nadir (τ_{NAD}) and NDVI index obtained over the 250 m MODIS pixel including the M-III vineyard (Fig. 3b). Relatively similar maximum values of τ_{NAD} were retrieved during the summer of all three years (maximum values of τ_{NAD} are close to 0.24 in 2010 and close to 0.22 in 2011 and 2012). During the winter period, after vine pruning and defoliation, values of τ_{NAD} close to 0.05 were retrieved for all three years. This latter value corresponds to the estimated value of the optical depth ($\tau_{\_STOCK}$) of vine stocks (Schwank et

al., 2012; Wigneron et al., 2012). Superimposed on the long term trend of τ_{NAD}, short-time changes in the time variations of τ_{NAD} can be noted. It is likely that these apparent fluctuations result from unaccounted for changes in the roughness conditions over the field as discussed in Patton and Hornbuckle (2013) and Jackson et al. (2012) for SMOS observations. It can be noted too that very low values of τ_{NAD} were retrieved during a short period of time in May of 2011 and 2012, just before the vine vegetation growth. We assumed that this could be caused by specific effects during this period related to soil roughness or to vegetation structure. For instance, this effect could be linked to lower roughness conditions in relation to field works in May. As the roughness parameterization is set as constant over the 3 year period, actual lower roughness conditions in the field would lead to retrievals of lower τ_{NAD} values and, to a lesser extent, higher SM values. Our field observations of roughness for the year 2012 (Fig. 1) are not accurate enough to confirm clearly this assumption but they seem to be leaning in that direction.

A maximum value of NDVI is reached in the middle of July (~ DoY 200): $NDVI_{MAX} \approx 0.45$ in 2010 and 2011 and $NDVI_{MAX} \approx 0.36$ in 2012. It is likely the lower value of $NDVI_{MAX}$ in 2012 can be related to the drier conditions during that year. In comparison with the year 2011, it seems that the very dry conditions during 2012 impact the NDVI values, but do not impact the time variations of τ_{NAD} considerably.

A scatter plot of the retrieved values of the optical depth τ_{NAD} versus the NDVI index is shown in Fig. 4. It can be seen that the results are generally consistent from one year to the other. One specific pattern can be noted in 2011; it corresponds to very low values of τ_{NAD} retrieved while vegetation is fully developed (NDVI ≈ 0.45), which was already discussed above.

3.3 Comparison of SM Retrievals

The retrieved values of SM from all retrieval methods presented in section 2 were compared to the reference SM values retrieved with the 2-P L-MEB method applied to the measurements performed during the years 2010-2012. A summary of this comparison is given in Table 4, in terms of coefficient of determination (R^2), bias (m^3/m^3), RMSE (m^3/m^3) and unbiased RMSE (ubRMSE, m^3/m^3) as defined by Entekhabi et al. (2010). To illustrate the

527 results, scatter plots of retrieved SM values versus 'reference' SM values are given for all
528 methods considered in this study (Fig. 5).

529 All five methods requiring a calibration step, e.g. SCA-V, SCA-H, 'Saleh' bi-angular, 'Saleh'
530 bi-polarization and 'Mattar' (the calibration was made using one year and the evaluation with
531 the two other years), provided SM retrievals that were in good agreement with the 'reference'
532 SM data (R^2 is generally higher than 0.90, and the RMSE is lower than 0.045 m^3/m^3). If we
533 consider the years used for calibration, best performances in terms of R^2 for all four methods
534 were obtained when year 2010 (corresponding to rather 'wet' conditions) was used for
535 calibration, while lower performances were obtained using the year 2012 (corresponding to
536 'very dry' conditions) for calibration. Results for the year 2011 are generally close to those
537 obtained for the year 2010. A closer inspection shows that both the SCA-V and the SCA-H
538 methods provide generally very similar performances in SM retrievals (the SCA-V method
539 providing a slightly better accuracy in terms of R^2, bias, RMSE and ubRMSE). The three
540 methods based on regression equations ('Saleh' bi-polarization, 'Saleh' bi-angular, and
541 'Mattar') provided very similar results too. Slightly lower performances were obtained for the
542 'Mattar' method (especially when using the year 2010 for calibration), while best
543 performances were obtained for 'Saleh bi-angular'. Considering the ubRMSE criteria, the
544 performances of the SCA and the regression methods were even closer. Except for the DCA
545 and LPRM algorithm, the ubRMSE is always around or below the target accuracy for SMAP
546 of 0.04 m^3/m^3. This is a direct consequence of the fact that values of the bias were found to be
547 higher for the SCA methods (bias $\approx$ 0.020 m^3/m^3) than for the regression methods (bias $\approx$
548 0.010 m^3/m^3).

549 As could be expected, results obtained from methods which did not require parameter
550 calibration (DCA and LPRM) provided results with a lower accuracy: the RMSE was similar
551 for both methods (RMSE $\approx$ 0.55 m^3/m^3), while slightly better R^2 values were obtained for
552 DCA (R^2 = 0.79) than for LPRM (R^2 = 0.725). For both methods, the bias in the retrievals
553 was found to be very low (bias = 0.021 m^3/m^3 for DCA, and bias = 0.013 m^3/m^3 for LPRM).

554 The scatter plots (Fig. 5) showing the comparison between retrieved SM values versus
555 'reference' SM values are given to illustrate these different results. For methods requiring
556 calibration (SCA-V, SCA-H, 'Saleh' bi-angular, 'Saleh' bi-polarization and 'Mattar'), we
557 used the year 2010 in Fig. 5 (this year provided best performances in terms of R^2). Note that

558 the number of data used in the comparison may vary from one approach to the other. This can
559 be explained by two reasons. First, for DCA and LPRM, the comparison was made over three
560 years (2010 - 2012), while it was made over two years (2011 -2012) for the other methods.
561 Second, retrieved SM values larger than the saturation value SM_{SAT} (SM_{SAT} = 0.5 m^3/m^3)
562 were removed in the comparison (a very low number of observations was concerned by this
563 filtering).

564 It can be seen that a very low bias was obtained generally. However, in wet conditions, the
565 methods LPRM and DCA provided underestimated SM values (for SM > 0.3 m^3/m^3); while
566 the 'Saleh' and 'Mattar' methods provided overestimated SM values (for SM > 0.2 m^3/m^3)
567 with respect to the reference SM. For DCA and LPRM (methods with do not require any
568 calibration), it can be seen that the SM retrieval performances are lower in a small SM
569 interval, for values of SM comprised between ~ 0.1 and 0.15 m^3/m^3. These SM conditions
570 generally correspond to periods of vegetation growth at the end of spring and of full
571 vegetation development in the summer period.

572

573 **4. Discussion and conclusion**

574 This study presents an inter-comparison of several SM retrieval methods based on a three year
575 data set of passive L-band microwave observations acquired over a vineyard site at the VAS
576 site.

577 A careful interpretation of the results should be made, and the results cannot be easily
578 generalized to operational applications for spaceborne sensors. We will discuss these different
579 aspects and the main conclusions of the study in the following. First, it is important to
580 consider that the results were obtained at the field scale and over only one type of vegetation
581 (a vineyard canopy) with some specific features (no litter layer, relatively low LAI and
582 biomass conditions, frequent agricultural practices leading to changes in soil roughness, etc.).
583 Several effects related to changes in the soil roughness conditions or in the vegetation
584 structure (in relation with the crop growth and the agricultural practices) may have a
585 significant impact on the results of the present study. It is likely that the impact of these
586 effects would average out and, therefore, become much less important if we had considered
587 larger footprints of spaceborne radiometric observations, including a large variety in the types
588 of vegetation (natural or cultivated canopies), in the soil conditions and in the agricultural

589 practices. For instance, specific effects related to the vegetation structure could be revealed
590 over the vineyard field and the values of optical depth for both polarizations ($\tau_H(\theta)$ and $\tau_V(\theta)$)
591 could not be considered as equal for that canopy type (Wigneron et al., 2012). This result has
592 frequently been obtained from *in situ* radiometric observations (Pardé et al., 2003, 2004;
593 Wigneron et al., 2004) but it has never been noted, to our knowledge, from spaceborne
594 observations. For instance, Owe et al. (2001) found that $\tau_V = \tau_H$ over test sites in the US over
595 a variety of land covers based on SMMR (Scanning Multichannel Microwave Radiometer)
596 observations at C-band. It is likely that these vegetation structure effects can be a limitation
597 for presented evaluation of the methods, which all assume $\tau_H = \tau_V$. So, several similar studies
598 based on *in situ* observations over a variety of vegetation types are required to provide a more
599 in-depth evaluation of the method performances.

600 It should be noted too that the performances of the different methods cannot be compared
601 directly as some methods had to be calibrated while some methods did not require any
602 parameter calibration step (DCA and LRPM). The two methods SCA-H and SCA-V, require
603 the calibration of the relationship between optical depth and a remotely sensed vegetation
604 index (NDVI); the three methods based on regression equations, 'Saleh bi-angular', 'Saleh bi-
605 polarization' and 'Mattar', require the calibration of three coefficients. This calibration step
606 could be done in the present study as we considered that a 'reference' data set describing the
607 time variations in SM and τ_{NAD} (and derived from multi-angular observations) was available
608 from the ELBARA-II tower-based observations. However, for operational spatial
609 applications, it is generally very difficult to obtain such a reference data set.

610 In spite of the limitations discussed above, some key results obtained in this study from
611 tower-based observations could be of value to future operational applications. It was found
612 that the two methods, which did not require any a priori calibration (DCA and LPRM) could
613 provide good SM retrievals and have relatively similar performances (R^2 ~ 0.72-0.79;
614 RMSE ~ 0.054-0.58 m^3/m^3) over the three year period. The methods requiring parameter
615 calibration (two parameters in SCA-H and SCA-V; three coefficients in the three regression
616 methods) provided results closer to the reference: for instance the R^2 coefficient increased
617 generally to values larger than 0.90 for all methods. The methods which require additional
618 information concerning the vegetation development (the NDVI variable is required in the
619 SCA-H, SCA-V and 'Mattar' algorithms) provided slightly lower performances when year
620 2012 was used for calibration. For that year the NDVI values were lower than for the two

other years (maximum NDVI values ≈ 0.45 in 2010 and 2011 and ≈ 0.36 in 2012), while the maximum values of τ_{NAD} were found to be relatively similar over all three years (≈ 0.22 – 0.24). It is likely that nonlinearities between τ_{NAD} and NDVI led to these slightly lower performances in SM retrievals for the year 2012 for the SCA and 'Mattar' algorithms.

In the present study, the computed performances are "optimal" performances as it is assumed that a good parameter calibration can be made from a SM data set which can be considered as a reference. This calibration step was possible in this study based on *in situ* tower-based observations obtained over a homogeneous vineyard field, but this step is much more complex for operational applications based on space borne sensors. Several options are possible to calibrate these different retrieval methods for spaceborne applications. For instance, the reference SM or τ_{NAD} values which are required in the calibration step can be estimated:

(i) from networks of *in situ* measurement sites such as SCAN in the USA (Schaefer et al., 2007), OZNET in Australia (Smith et al., 2012) or SMOSMANIA in France (Albergel et al., 2012), etc. Then, based on results obtained over a variety of soil and vegetation conditions, a look up table providing the calibrated parameters as function of the land cover types can be built.

(ii) from model re-analyses (ERA-Interim (Dee et al., 2011) or MERRA Land (Reichle et al., 2012) for instance), in regions where the simulated SM values can be considered to be accurate. As mentioned above, in a second step, a look up table can be built for a variety of land covers.

(iii) by combining observations from different remote sensing sensors. For instance, the estimation of optical depth τ_{NAD} retrieved from SMOS or other satellites (e.g. AMSR-2) could be used to calibrate the vegetation parameters required in the SCA-H and SCA-V algorithms (Lawrence et al., 2014).

Future work will consider these different options to evaluate the retrieval capabilities of the different methods requiring calibration (SCA, 'Saleh' or Mattar') for operational applications based on spaceborne sensors.

650

651 **Acknowledgments**

652

653 This study received financial support from the TOSCA program of CNES (Centre National
654 d'Etudes Spatiales, France), the Spanish National Program on Space Research (MIDAS-5 and -
655 6 Projects) and ESA (European Space Agency) in the framework of the cal/val activities of
656 the SMOS mission. The MODIS MOD13Q1 data were obtained through the online Data Pool
657 at the NASA Land Processes Distributed Active Archive Center (LP DAAC), USGS/Earth
658 Resources Observation and Science (EROS) Center, Sioux Falls, South Dakota
659 (http://lpdaac.usgs.gov/get_data). The CATDS data were obtained from the "Centre Aval de
660 Traitement des Données SMOS" (CATDS), operated for the "Centre National d'Etudes
661 Spatiales" (CNES, France) by IFREMER (Brest, France).

662

663 **References**

664 Albergel, C., Zakharova, E., Calvet, J.-C., Zribi, M., Pardé, M., Wigneron, J.-P., Novello, N.,
665 Kerr, Y., Mialon, A., Fritz, N. (2011). A first assessment of the SMOS data in southwestern
666 France using *in situ* and airborne soil moisture estimates: the CAROLS airborne campaign.
667 *Remote Sensing of Environment, 115*, 2718-2728.

668 Al Bitar, A., Leroux, D., Kerr, Y. H., Merlin, O., Richaume, P., Sahoo, A., Wood, E. F.
669 (2012). Evaluation of SMOS Soil Moisture products over continental US using the
670 SCAN/SNOTEL network. *IEEE Transactions on Geoscience and Remote Sensing.* 50(5),
671 1572 – 1586.

672 Berthon, L., Mialon, A., Al Bitar, A., Cabot, F. and Kerr, Y.H. (2012). SMOS CATDS Level
673 3 Soil Moisture Products. *Proceedings of 2012 EGU General Assembly*, Vienna, April 2012.

674 Bindlish, R., Jackson, T., Cosh, M., Zhao, T. & O'Neill, P. (2014). Global Soil Moisture from
675 the Aquarius Satellite: Description and Initial Assessment. *IEEE Geoscience and Remote*
676 *Sensing Letters*, submitted.

677 De Lannoy, G. J. M., Reichle, R. H. & Pauwels, V. R. N. (2013). Global Calibration of the
678 GEOS-5 L-Band Microwave Radiative Transfer Model over Nonfrozen Land Using SMOS
679 Observations. *Journal of Hydrometeorology*, 14, 765-785.

680 Calvet, J.-C., Wigneron, J.-P., Walker, J., Karbou, F., Chanzy, A. & Albergel, C. (2011).
681 Sensitivity of passive microwave observations to soil moisture and vegetation water content:
682 from L-band to W-band. *IEEE Transactions on Geoscience and Remote Sensing.* 49, 4, 1190-
683 1199.

684 Cano A., Saleh, K., Wigneron, J.-P., Antolín, C., Balling, J. E., Kerr, Y. H., Kruszewski, A.,
685 Millán-Scheiding, C., Schmidl Søbjærg, S., Skou, N., López-Baeza, E. (2010). The SMOS
686 Mediterranean Ecosystem L-Band characterisation EXperiment (MELBEX-I) over natural
687 shrubs, *Remote Sensing of Environment, 114(4*), 844-853.

688 Chung, D., de Jeu, R.A.M., Dorigo, W., Hahn, S., Melzer, T., Parinussa R.M. et al. (2013).
689 ESA CCI soil moisture algorithm theoretical baseline document version 1, pp. 36–44.
690 http://www.esa-soilmoisture-cci.org/

691 Dee, D. P., Uppala, S. M., Simmons, A. J., Berrisford, P., Poli, P., Kobayashi, S., et al.
692 (2011), The ERA-Interim reanalysis: configuration and performance of the data assimilation
693 system, *Quarterly Journal of the Royal Meteorological Society, 137*, 553–597.
694 doi: 10.1002/qj.828.

695 de Jeu, R., Holmes, T., Panciera, R. & Walker, J. (2009). Parameterization of the Land
696 Parameter Retrieval Model for L-Band Observations Using the NAFE'05 Data Set. *IEEE*
697 *Geoscience and Remote Sensing Letters*, 6 (4), 630-634.

698 de Rosnay P., Calvet, J.-C. , Kerr, Y., Wigneron, J.-P., Lemaître, F.et al. (2006). SMOSREX:
699 A Long Term Field Campaign Experiment for Soil Moisture and Land Surface Processes
700 Remote Sensing. *Remote Sensing of Environment*, 102, 377-389.

701 Dobson, M. C., Ulaby, F. T., Hallikainen, M. T., & El-Reyes, M. A. (1985). Microwave
702 dielectric behavior of wet soil- Part II: Dielectric mixing models. *IEEE Transactions on*
703 *Geoscience and Remote Sensing.*, 23, 35-46.

704 Entekhabi, D., Reichl, R. H., Koster R. D., Crow, W. T. (2010). Performance Metrics for Soil
705 Moisture Retrievals and Application Requirements. *Journal of Hydrometeorology*, 11, 832-
706 840.

707 Entekhabi, D., Njoku, E., O'Neill, P., Kellogg, K. et al. (2010). The Soil Moisture Active
708 Passive (SMAP) Mission. *Proceedings of the IEEE*, 98, 5.

709 Grant, J.P., Saleh, K., Wigneron, J.-P., Guglielmetti, M., Kerr,Y., Schwank, M., Skou, N. &
710 Van de Griend, A.A. (2008). Calibration of the L-MEB model over a coniferous and a
711 deciduous forest. *IEEE Transactions on Geoscience and Remote Sensing*, *46(3)*, 808-818.
712 Hornbuckle, B K. & England, A. W. (2004). Radiometric Sensitivity to Soil Moisture at 1.4
713 GHz Through a Corn Crop at Maximum Biomass. *Water Ressources Research*, 40(10): doi:
714 10.1029/2003WR002931.

715 Jackson, T. J., & Schmugge, T. J. (1991). Vegetation effects on the microwave emission of
716 soils. *Remote Sensing of Environment*, *36*, 203-212.

717 Jackson, T. J., Le Vine, D. M., Swift, C. T., Schmugge, T. J., & Schiebe, F. R. (1995).
718 Large area mapping of soil moisture using the ESTAR passive microwave radiometer in
719 Washita'92. *Remote Sensing of Environment*, *53*, 27-37.

720 Jackson, T. J., Bindlish, R., Cosh, M. H., Zhao, T., Starks, P. J., Bosch, D. D., Seyfried, M. S.,
721 Moran, M. S., Kerr, Y., & Leroux, D. (2012). Validation of Soil Moisture and Ocean Salinity
722 (SMOS) soil moisture over watershed networks in the U.S. *IEEE Transactions on Geoscience*
723 *and Remote Sensing,* 50, 5, 1530-1543.

724 Juglea, S., Kerr, Y., Mialon, A. Wigneron, J.-P., Lopez-Baeza, E., et al. (2010). Modelling
725 soil moisture at SMOS scale by use of a SVAT model over the Valencia Anchor Station.
726 *Hydrol. Earth Syst. Sci.*, doi:10.5194/hess-14-831-2010, 14, 831-846.

727 Kerr, Y. H., Waldteufel, P., Wigneron, J.-P., Font, J., & Berger, M., (2001). Soil Moisture
728 Retrieval from Space: The Soil Moisture and Ocean Salinity (SMOS) Mission. *IEEE*
729 *Transactions on Geoscience and Remote Sensing*, *39*(8), 1729-1735.

730 Kerr Y. H., Waldteufel, P., Richaume, P., Wigneron, J.-P. et al. (2012). The SMOS soil
731 moisture retrieval algorithm', *IEEE Transactions on Geoscience and Remote Sensing*, 50(5),
732 1384-1403.

733 Kurum, M., Lang, R. H., O'Neill, P. E., Joseph, A. T., Jackson, T. J. , & Cosh, M. H. (2009).
734 L-Band Radar Estimation of Forest Attenuation for Active/Passive Soil Moisture Inversion.
735 *IEEE Transactions on Geoscience and Remote Sensing*, 47, 9, 3026-3040.

736 Kurum, M. (2013). Quantifying scattering albedo in microwave emission of vegetated terrain.
737 *Remote Sensing of Environment*, *129*, 66-74.

738 Lawrence, H., Wigneron, J-P, Demontoux, F., Mialon, A., & Kerr, Y. H. (2013). Evaluating
739 the semi-empirical H − Q model used to calculate the emissivity of a rough bare soil, with a
740 numerical modelling approach. *IEEE Transactions on Geoscience and Remote Sensing*, 51, 7,
741 4075-4084.
742 Lawrence H., Wigneron, J.-P., Lopez-Baeza, E. et al. (2014). Comparison between SMOS
743 Vegetation Optical Depth products and MODIS Vegetation Indices over the USA. *Remote*
744 *Sensing of Environment, 140*, 396 – 406, 2014.

745 Le Vine, D. M., Lagerloef, G. S., & Torrusio, S. E. (2010). Aquarius and remote sensing of
746 sea surface salinity from space. *Proceedings of the IEEE*, 98(5), 688-703.

747 Liu, S. F., Liou, Y.-A., Wang, W. J. Wigneron, J.-P. & Lee, J. B. (2002). Retrieval of crop
748 biomass and soil moisture from measured 1.4 and 10.65 brightness temperatures. *IEEE*
749 *Transactions on Geoscience and Remote Sensing*, 40(6), 1260-1268.

750 Luo, Y., Feng, X., Houser, P., Anantharaj, V., Fan, X. , De Lannoy, G. et al. (2013). Potential
751 soil moisture products from the aquarius radiometer and scatterometer using an observing
752 system simulation experiment. *Geosci. Instrum. Method. Data Syst.*, 2, 113–120.

753 Mattar, C., Wigneron, J.-P., Sobrino, J. A., Novello, N., Calvet, J.-C., Albergel, C.,
754 Richaume, P., Mialon, A., Guyon, D., Jiménez Muñoz, J.C. & Kerr, Y. (2012). A combined
755 optical-microwave method to retrieve soil moisture over vegetated areas. *IEEE Transactions*
756 *on Geoscience and Remote Sensing*, 50(5), 1404-1413.

757 Meesters, A. G. C. A., de Jeu, R. A. M. et al. (2005). Analytical derivation of the vegetation
758 optical depth from the microwave polarization difference index. *Geoscience and Remote*
759 *Sensing Letters*, 2(2), 121-123.

760 Mialon, A., de Rosnay, P., Wigneron, J.-P., Escorihuela, M.-J. & Kerr, Y. H. (2012).
761 Evaluating the L-MEB model from long term microwave measurements over a rough field,
762 SMOSREX 2006. *IEEE Transactions on Geoscience and Remote Sensing*, 50(5), 1458-1467.

763 Mialon A., Al Bitar, A., Berthon, L. et al. (2012). Validation of SMOS Level 3 soil moisture',
764 *IEEE International Geoscience and Remote Sensing Symposium*, IGARSS'2012, 22-27 July
765 2012, Munich, Germany.

766 Mo, T., Choudhury, B.J., Schmugge, T.J., Wang J.R., & Jackson, T.J. (1982). A model for
767 microwave emission from vegetation-covered fields. *J. of Geophysical Research*, 87,
768 11.229-11.237.

769 MODIS (2010). NASA Land Processes Distributed Active Archive Center (LP DAAC).
770 MOD13Q1 collection 5. USGS/Earth Resources Observation and Science (EROS) Center,
771 Sioux Falls, South Dakota.

772 Njoku, E.G., Jackson, T.J., Lakshmi, V., Chan, T.K. & Nghiem, S.V. (2003). Soil moisture
773 retrieval from AMSR-E. *IEEE Transactions on Geoscience and Remote Sensing*, 41(.2), 215-
774 229.

O'Neill, P., Chan, S., Njoku, E., Jackson, T. & Bindlish R., Soil Moisture Active Passive (SMAP) Algorithm Theoretical Basis Document (ATBD), SMAP Level 2 & 3 Soil Moisture (Passive), (L2_SM_P, L3_SM_P), Initial Release, v.1, http://smap.jpl.nasa.gov/files/smap2/L2&3_SM_P_InitRel_v1_filt2.pdf

Owe, M., de jeu, R., & Holmes, T. (2008). Multisensor historical climatology of satellite-derived global land surface moisture. *Journal of Geophysical Research-Earth Surface, 113*, F01002

Panciera, R., Walker, J. P., Kalma, J. D., Kim, E. J., Saleh, K., & Wigneron, J.-P. (2009). Evaluation of the SMOS L-MEB passive microwave soil moisture retrieval algorithm. *Remote Sensing of Environment,* 113, 435–444.

Pardé, M., Wigneron, J.-P., Chanzy, A., Waldteufel, P., Kerr, Y.& Huet, S. (2003). Retrieving surface soil moisture over a wheat field: Comparison of different methods. *Remote Sensing of Environment*, 87, 334-344.

Pardé, M, Wigneron, J-P, Chanzy, A., Kerr, Y., Calvet, J.C., Waldteufel, P., Schmidl, S. & Skou, N. (2004). N-Parameter retrievals from L-band microwave measurements over a variety of agricultural crops, *IEEE Transactions on Geoscience and Remote Sensing*, 42(6), 1168-1178.

Parinussa, R. M., Holmes, T. R. H., Yilmaz, M. T. & Crow, W. T. (2011). The impact of land surface temperature on soil moisture anomaly detection from passive microwave observations. *Hydrol. Earth Syst. Sci.*, 15, 3135–3151.

Parrens, M., Zakharova, E., Lafont, S., Calvet, J.-C., Kerr, Y., Wagner, W., && Wigneron, J.-P. (2012). Comparing soil moisture retrievals from SMOS and ASCAT over France. *Hydrol. Earth Syst. Sci.*, 16, 423-440, doi:10.5194/hess-16-423-2012.

Pellarin, T., Mialon, A., Biron, R. et al. (2013). Two years of L-band radiometry over a moutainous region: topography, snow and freezing soil issues. *IEEE International Geoscience and Remote Sensing Symposium*, IGARSS 2013, 21-26 July, Melbourne.

Rodriguez-Fernandez, NJ, Aires, F, Richaume, P, Prigent, C, & Kerr, Y.H. "Soil Moisture retrieval from SMOS observations using neural networks", 2013, *to be submitted*

803 Reichle, R. H., Koster, R. D., De Lannoy, G. J. M., et al. (2011). Assessment and
804 enhancement of MERRA land surface hydrology estimates, *J. Climate*, 24, 6322-6338,
805 doi:10.1175/JCLI-D-10-05033.1.

806 Saleh, K., Wigneron, J.-P., de Rosnay, P., Calvet, J.-C. & Kerr, Y. (2006). Semi-empirical
807 regressions at L-band applied to surface soil moisture retrievals over grass, *Remote Sensing of*
808 *Environment, 101*, 415-426.

809 Schaefer, G. L., Cosh, M. H., and Jackson, T. J. (2007). The USDA Natural Resources
810 Conservation Service Soil Climate Analysis Network (SCAN). *Journal of Atmospheric and*
811 *Oceanic Technology*, 24(12), 2073-2077.

812 Schlenz, F., Fallmann, J., Marzahn, P., Loew, A. & Mauser, M. (2012). Characterization of
813 Rape Field Microwave Emission and Implications to Surface Soil Moisture Retrievals.
814 *Remote Sensing*, 4, 247-270; doi:10.3390/rs4010247.

815 Schwank, M., Wiesmann, A. et al. (2010). "ELBARA II, An L-Band Radiometer System for
816 Soil Moisture Research. *Sensors*, MDPI 10: 584-612.

817 Schwank M, Wigneron, J.-P., Lopez-Baeza, E., Völksch, I., Mätzler, C. & Kerr, Y. (2012). 'L-
818 Band Radiative Properties of Vine Vegetation at the MELBEX III SMOS Cal/Val Site. *IEEE*
819 *Transactions on Geoscience and Remote Sensing*, 50(5), 1587-1601.

820 Smith, A. B., Walker, J. P., Western, A. W., Young, R. I., Ellett, K. M., Pipunic, R., Grayson,
821 R., Siriwidena, L., Chiew, F., and Richter, H. (2012). The Murrumbidgee soil moisture
822 monitoring network data set. Water Resources Research, 48, W07701.1–6.

823 Wigneron, J. -P., Chanzy, A., Calvet, J. -C., & Bruguier, N. (1995). A simple algorithm to
824 retrieve soil moisture and vegetation biomass using passive microwave measurements over
825 crop fields. Remote Sensing of Environment, 51(3), 331–341.

826 Wigneron, J.-P., Waldteufel, P., Chanzy, A., Calvet, J.-C., & Kerr, Y. (2000). Two-D
827 microwave interferometer retrieval capabilities of over land surfaces (SMOS Mission).
828 *Remote Sens. Environ.*, *73*, 270-282.

829 Wigneron J.-P., Calvet, J.-C., de Rosnay, P., Kerr, Y., Waldteufel, P., Saleh, K. et al. (2004).
830 Soil Moisture Retrievals from Bi-Angular L-band Passive Microwave Observations. *IEEE*
831 *Trans. Geosc. Remote Sens. Let.*, 1(4), 277-281.

832 Wigneron, J.-P., Kerr, Y., Waldteufel, P., Saleh, K., Escorihuela, M.-J., Richaume, P.,
833 Ferrazzoli, P., de Rosnay, P., Gurney, R., Calvet, J.-C., Guglielmetti, M., Hornbuckle, B.,
834 Matzler, C., Pellarin, T., & Schwank, M. (2007). L-band Microwave Emission of the
835 Biosphere (L-MEB) Model: description and calibration against experimental data sets over
836 crop fields. *Remote Sensing of Environment*, *107(4)*, 639–655.

837 Wigneron, J-P, Schwank, M., Lopez Baeza, E., et al. (2012). First evaluation of the SMOS
838 observations over the VAS site in the Mediterranean region. *Remote Sensing of Environment*,
839 124, 26–37.

840

841

842 **Table 1.**

843 L-MEB soil and vegetation parameters over the M-III vineyard (VAS site). All these parameters,
844 except tt_H and tt_V which are specific to L-MEB, are valid for the other SM retrieval methods.

	Unit	Value or used Model
Soil dielectric permittivity (ε_G)	(-)	Mironov et al. (2012)
Clay fraction	(-)	0.26 (in situ measurements; Juglea et al., 2010)
T_G=T_C=T_{GC}	K	ECMWF ERA Interim temperature ($T_{E\text{-}07}$)
H_R	(-)	0.6060 (calibrated, Lawrence et al., 2013)
Q_R	(-)	0.0303 (calibrated, Lawrence et al., 2013)
N_{RH}	(-)	0
N_{RV}	(-)	0
tt_H	(-)	1
tt_V	(-)	Free parameter in the retrieval process
ω	(-)	0.02
τ	(-)	Free parameter in the retrieval process
SM	m^3/ m^3	Free parameter in the retrieval process

845

846

847 **Table 2.**

848 Input variables required in the different retrieval algorithms

849

Algorithm	Input variables
SCA-H	$T_{BH}(\theta=40°)$
	ECMWF temperature ($T_{E\text{-}07}$)
	NDVI
SCA-V	$T_{BV}(\theta=40°)$
	ECMWF temperature ($T_{E\text{-}07}$)
	NDVI
DCA	$T_{BH}(\theta=40°)$, $T_{BV}(\theta=40°)$
	ECMWF temperature ($T_{E\text{-}07}$)
LPRM	$T_{BH}(\theta=40°)$, $T_{BV}(\theta=40°)$
	ECMWF temperature ($T_{E\text{-}07}$)
'Saleh' bi-polarization	$T_{BH}(\theta=40°)$, $T_{BV}(\theta=40°)$
	ECMWF temperature ($T_{E\text{-}07}$)
'Saleh', bi-angular	$T_{BH}(\theta=30°)$, $T_{BH}(\theta=50°)$
	ECMWF temperature ($T_{E\text{-}07}$)
'Mattar'	$T_{BH}(\theta=40°)$
	ECMWF temperature ($T_{E\text{-}07}$)
	NDVI

850

851

852

853 **Table 3.**

854 Calibrated parameters of the different retrieval algorithms: one year (2010, 2011 or 2012) is used for
855 calibration; the two other years are used for validation

856 **SCA H/V,** $T_{BH}(\theta=40)$ or $T_{BV}(\theta=40)$

Calibration	b	Stemfactor
2010	0.61679	0.20874
2011	0.31756	0.44014
2012	0.92819	0.05840

857 **'Saleh bi-angular',** $T_{BH}(\theta=30)$, $T_{BH}(\theta=50)$

Calibration	a_0	a_1	a_2
2010	1.4171	-0.3560	0.8374
2011	1.0972	-0.2806	0.2613
2012	2.2857	-1.5674	0.1300

858

859 **'Saleh bi-polarization',** $T_{BH}(\theta=40)$, $T_{BV}(\theta=40)$

Calibration	b_O	b_1	b_2
2010	0.3524	0.7734	1.1401
2011	0.2595	0.6208	0.4879
2012	-0.3914	1.1927	0.7263

860 **'Mattar',** $T_{BH}(\theta=40)$

Calibration	c_0	c_1	C_2
2010	1.2530	0.9491	0.9147
2011	0.9844	0.5748	0.3702
2012	1.0954	2.6578	0.0183

861
862

863

Table 4.

Performances of the different SM retrieval algorithms in terms of coefficient of determination (R^2), bias (m^3/m^3), RMSE (m^3/m^3) and ubRMSE (m^3/m^3). For SCA-H, SCA-V, 'Saleh bi-angular', 'Saleh bi-polarization' and 'Mattar', one year (2010, 2011 or 2012) is used for calibration; the two others are used for validation. For LPRM and DCA, no calibration is required.

Method	Calibration	Validation	R^2	Bias (m^3/m^3)	RMSE (m^3/m^3)	ubRMSE (m^3/m^3)
SCA-H	2010	2011, 2012	0.915	-0.025	0.050	0.043
	2011	2010, 2012	0.905	-0.041	0.054	0.035
	2012	2010, 2011	0.852	-0.020	0.056	0.052
SCA-V	2010	2011, 2012	0.928	-0.014	0.035	0.032
	2011	2010, 2012	0.919	-0.024	0.040	0.032
	2012	2010, 2011	0.861	-0.010	0.045	0.043
DCA			0.789	0.021	0.054	0.050
LPRM			0.725	0.013	0.058	0.056
Saleh Bi-angular	2010	2011, 2012	0.950	0.004	0.037	0.037
	2011	2010, 2012	0.941	0.007	0.028	0.027
	2012	2010, 2011	0.934	0.009	0.036	0.035
Saleh Bi-polarization	2010	2011, 2012	0.946	0.010	0.040	0.039
	2011	2010, 2012	0.924	-0.001	0.031	0.031
	2012	2010, 2011	0.920	0.004	0.033	0.033
Mattar	2010	2011, 2012	0.946	0.009	0.041	0.040
	2011	2010, 2012	0.927	-0.001	0.030	0.030
	2012	2010, 2011	0.869	0.017	0.048	0.045

871 **Figure Captions**

872 **Fig. 1** Temporal variations in the standard deviation of soil surface heights S_D and correlation
873 length L_C estimated from measurements during seven days in 2012 performed at the M-III
874 vineyard field. The annual mean values are $\langle S_D \rangle = 2.2$ cm, $\langle L_C \rangle = 6.2$ cm.

875 **Fig. 2.** Time–series of measured ELBARA-II T_B over the M-III vineyard during three years
876 (2010-2012) at H ('o') and V ('x') polarizations and at the observation angle $\theta = 40°$. The T_B
877 data are acquired ~ every 30 minutes but only data measured at 6 am are shown. Diurnal
878 precipitation P is represented with vertical lines

879 **Fig. 3.** Soil moisture SM (a) and optical depth τ_{NAD} (b) retrieved with the multiangular 2-P L-
880 MEB method applied to the measurements at the M-III site. The diurnal retrievals are shown
881 for 6 am and 6 pm, respectively. These retrieved values are considered as a reference in this
882 study. Diurnal precipitation is represented with vertical lines. In Fig 3b, the time-series of
883 NDVI index obtained over the 250 m MODIS pixel including the M-III vineyard is shown.

884 **Fig. 4.** Scatter plot of retrieved values of the optical depth τ_{NAD}, retrieved with the
885 multiangular 2-P L-MEB method, versus the NDVI index obtained over the 250m MODIS
886 pixel including the M-III vineyard. Retrieved values of τ_{NAD} computed at 6 am and 6 pm are
887 used.

888 **Fig. 5.** Scatter plots of the retrieved SM values versus the reference SM values for all
889 methods: SCA-H (a), SCA-V (b), DCA (c), LPRM (d), 'Saleh' bi-angular (e), 'Saleh' bi-
890 polarization (f) and 'Mattar' (g). Retrieved values of SM are computed at 6 am and 6 pm. In
891 Fig. 5a-b-e-f-g, retrieved values of SM for years 2011 and 2012 are shown (the year 2010 was
892 used for calibration). In Fig. 5c-d (for DCA and LPRM) retrieved values of SM for years
893 2011, 2012 and 2013 are shown (no calibration was required).

894

Fig. 1 Temporal variations in the standard deviation of soil surface heights S_D and correlation length L_C estimated from measurements during seven days in 2012 performed at the M-III vineyard field. The annual mean values are $\langle S_D \rangle = 2.2$ cm, $\langle L_C \rangle = 6.2$ cm.

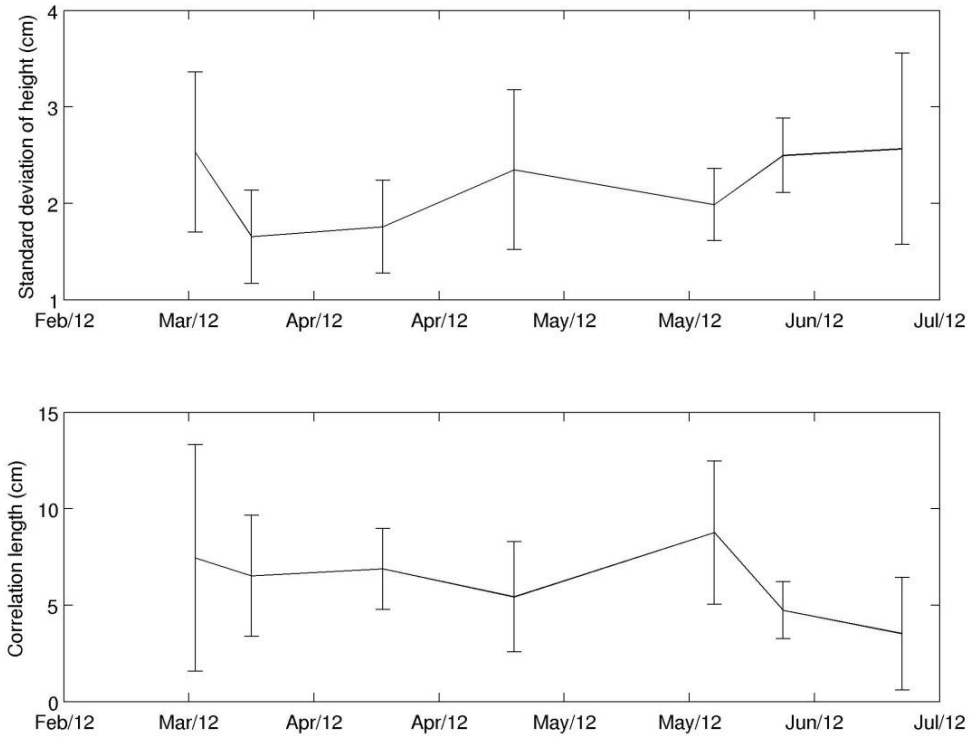

900 **Fig. 2.** Time–series of measured ELBARA-II T_B over the M-III vineyard during three years
901 (2010-2012) at H ('o') and V ('x') polarizations and at the observation angle $\theta = 40°$. The T_B
902 data are acquired ~ every 30 minutes but only data measured at 6 am are shown. Diurnal
903 precipitation P is represented with vertical lines.

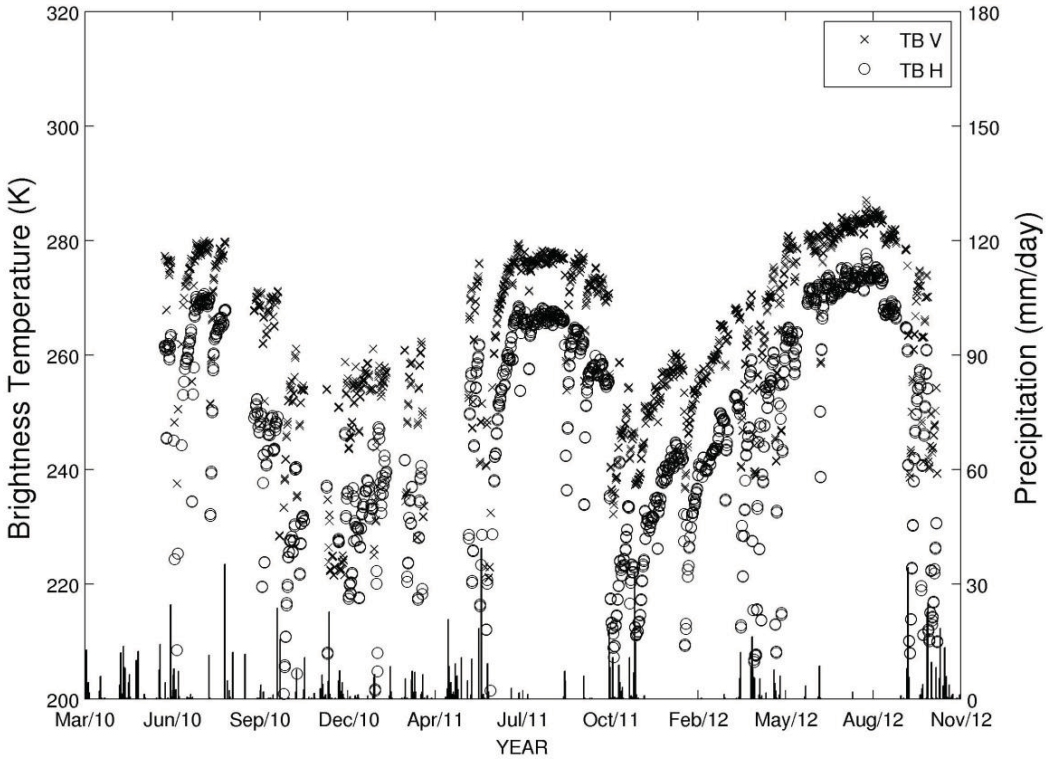

904

905 **Fig. 3.** Soil moisture SM (a) and optical depth τ_{NAD} (b) retrieved with the multiangular 2-P L-
906 MEB method applied to the measurements at the M-III site. The diurnal retrievals are shown
907 for 6 am and 6 pm, respectively. These retrieved values are considered as a reference in this
908 study. Diurnal precipitation is represented with vertical lines. In Fig 3b, the time-series of
909 NDVI index obtained over the 250 m MODIS pixel including the M-III vineyard is shown.

910 **a)**

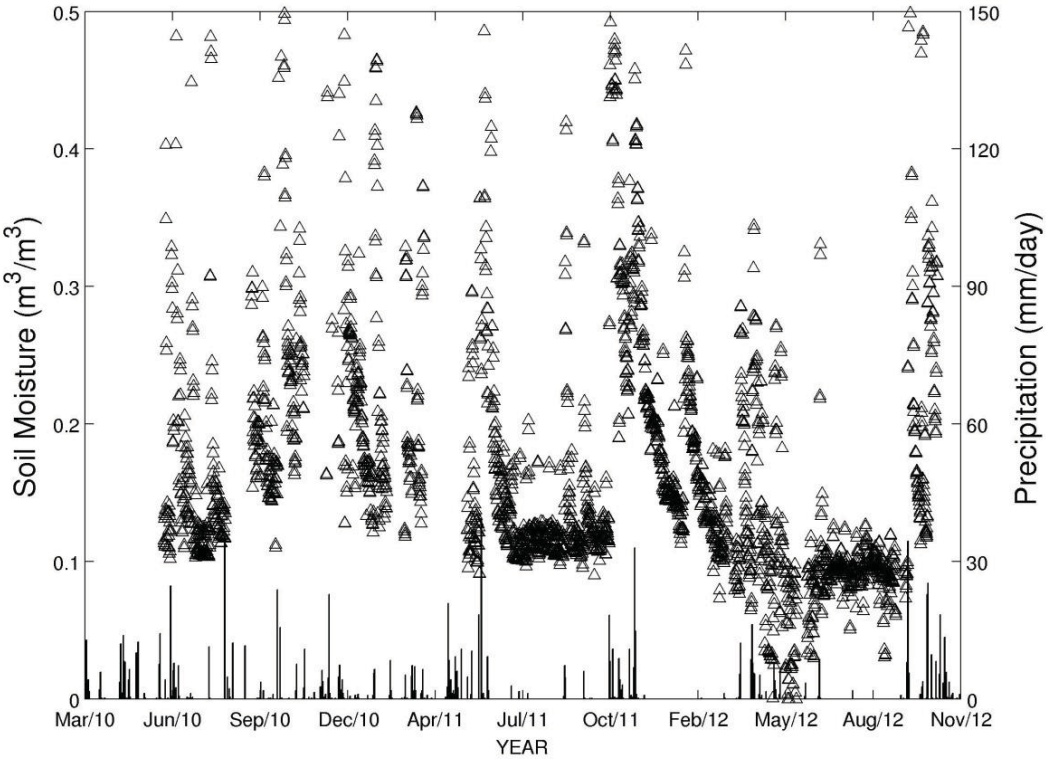

911

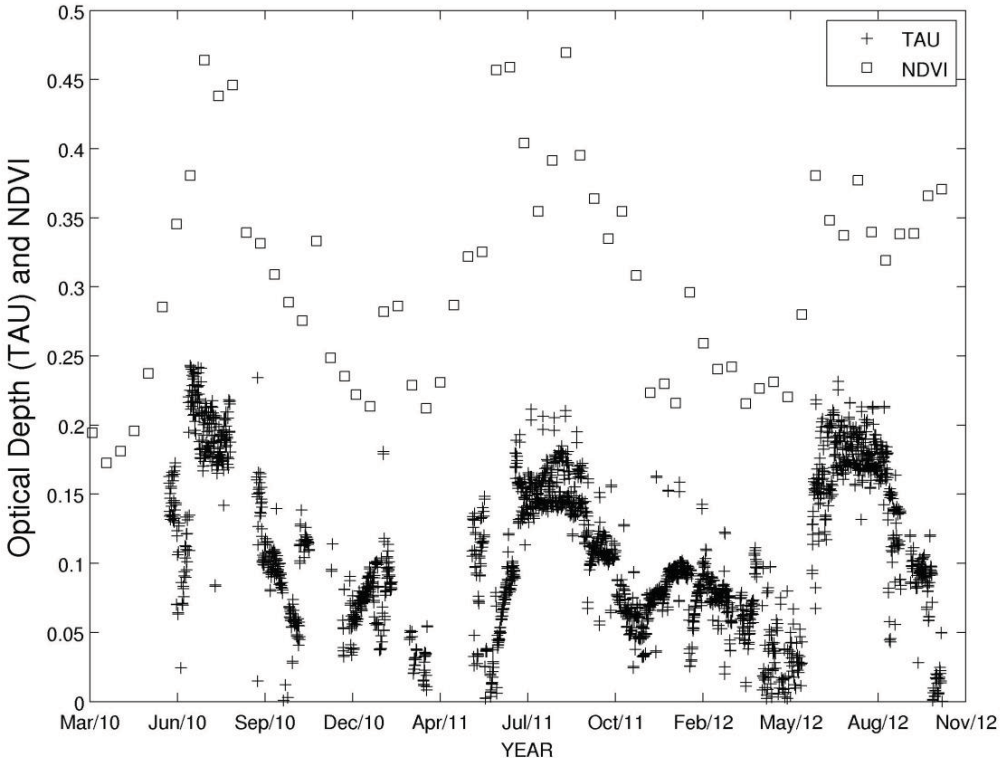

912

913 **b)**

914

915

Fig. 4. Scatter plot of retrieved values of the optical depth τ_{NAD}, retrieved with the multiangular 2-P L-MEB method, versus the NDVI index obtained over the 250m MODIS pixel including the M-III vineyard. Retrieved values of τ_{NAD} computed at 6 am and 6 pm are used.

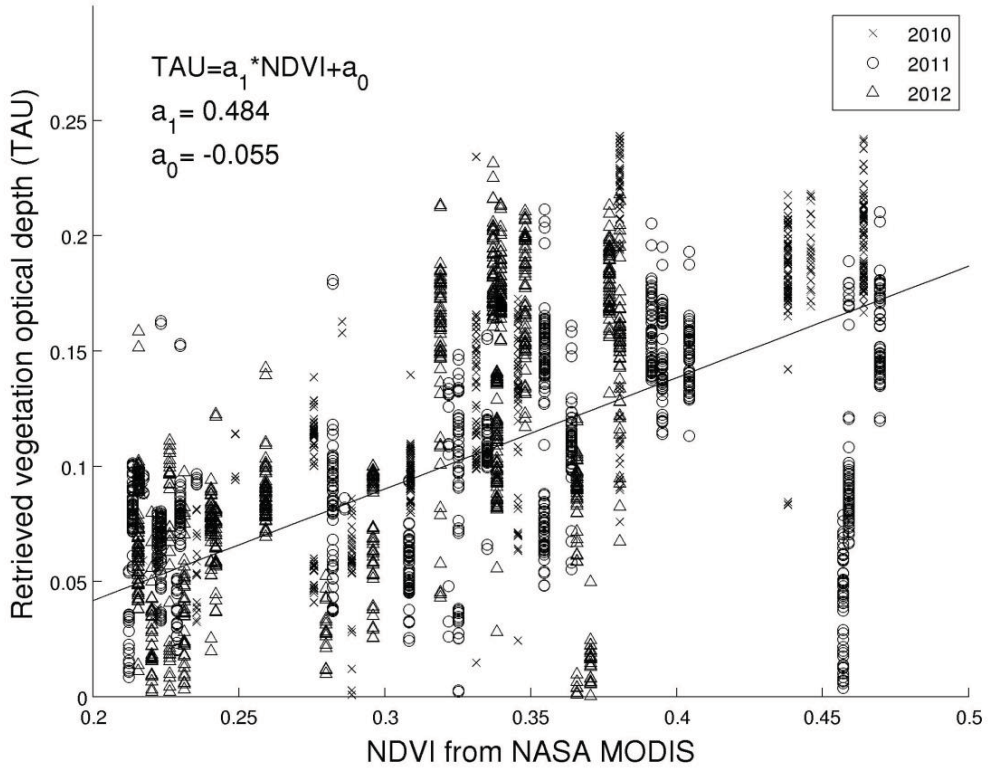

Fig. 5. Scatter plots of the retrieved SM values versus the reference SM values for all methods: SCA-H (a), SCA-V (b), DCA (c), LPRM (d), 'Saleh' bi-angular (e), 'Saleh' bi-polarization (f) and 'Mattar' (g). Retrieved values of SM are computed at 6 am and 6 pm. In Fig. 5a-b-e-f-g, retrieved values of SM for years 2011 and 2012 are shown (the year 2010 was used for calibration). In Fig. 5c-d (for DCA and LPRM) retrieved values of SM for years 2011, 2012 and 2013 are shown (no calibration was required).

a)

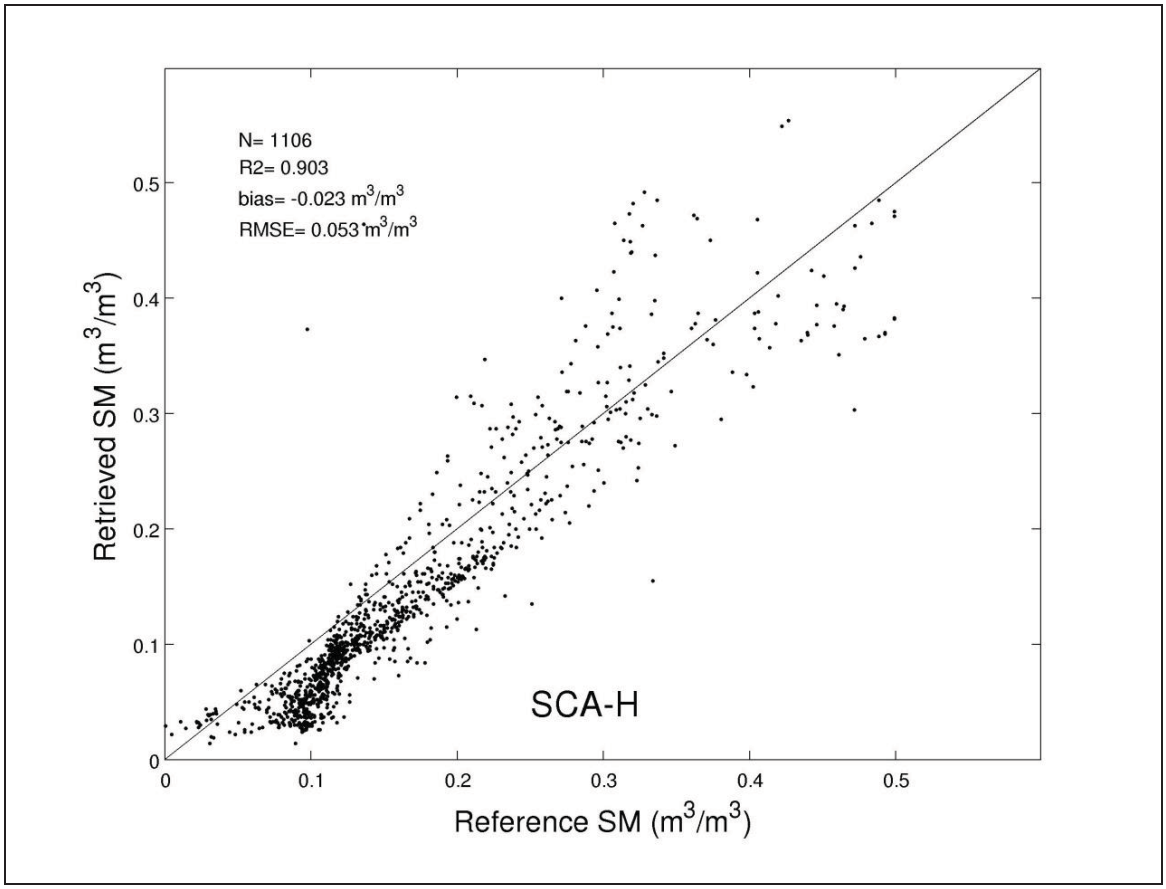

931 b)

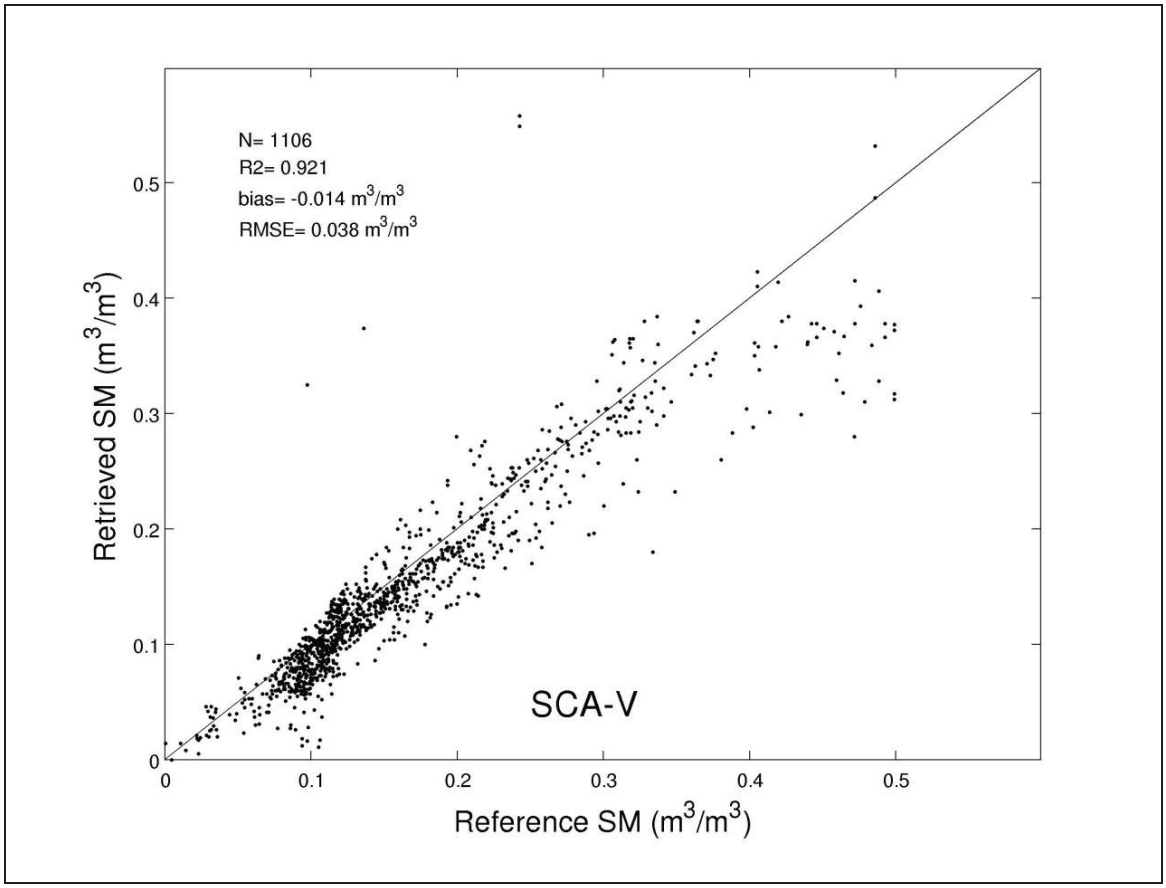
N= 1106
R2= 0.921
bias= -0.014 m3/m3
RMSE= 0.038 m3/m3
SCA-V
Retrieved SM (m3/m3)
Reference SM (m3/m3)
0
0.1
0.2
0.3
0.4
0.5

932

933

934 c)

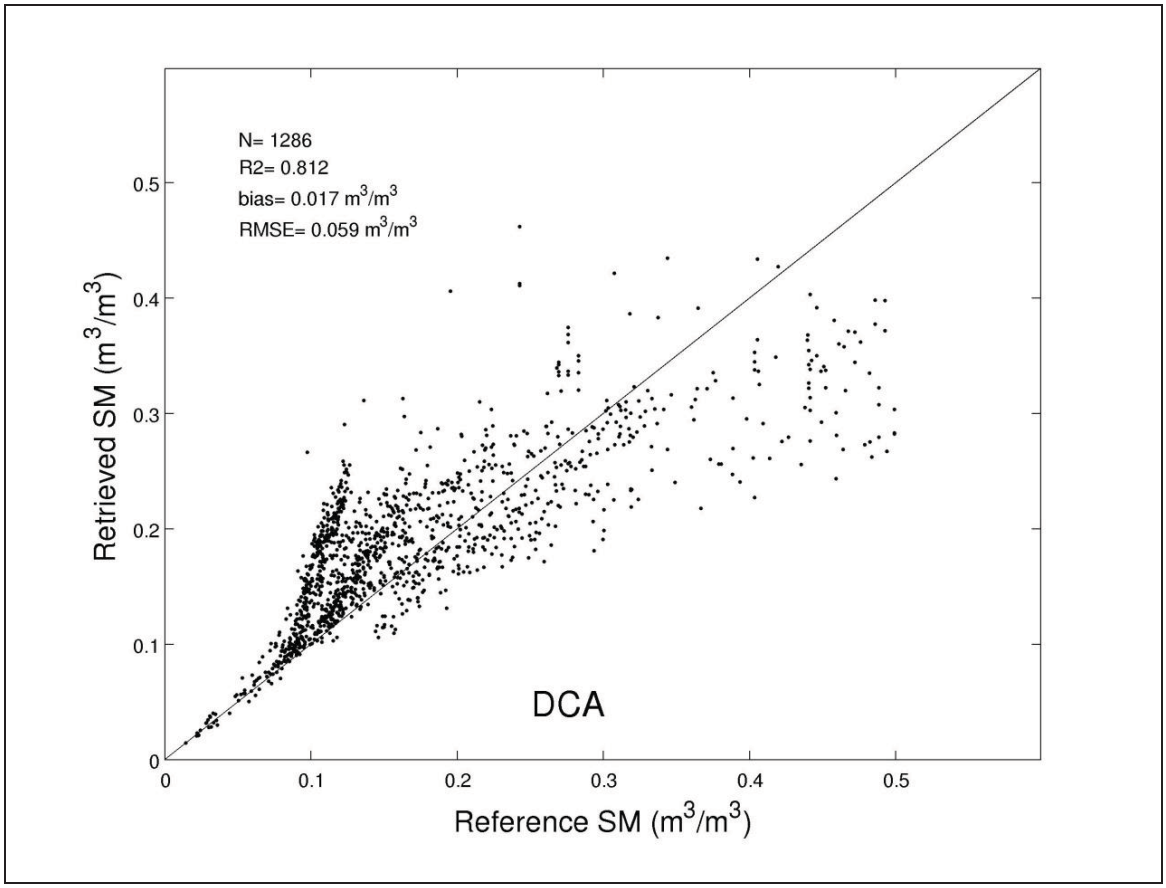
N= 1286
R2= 0.812
bias= 0.017 m3/m3
RMSE= 0.059 m3/m3
DCA
Retrieved SM (m3/m3)
Reference SM (m3/m3)
0
0.1
0.2
0.3
0.4
0.5

935

936

937 d)

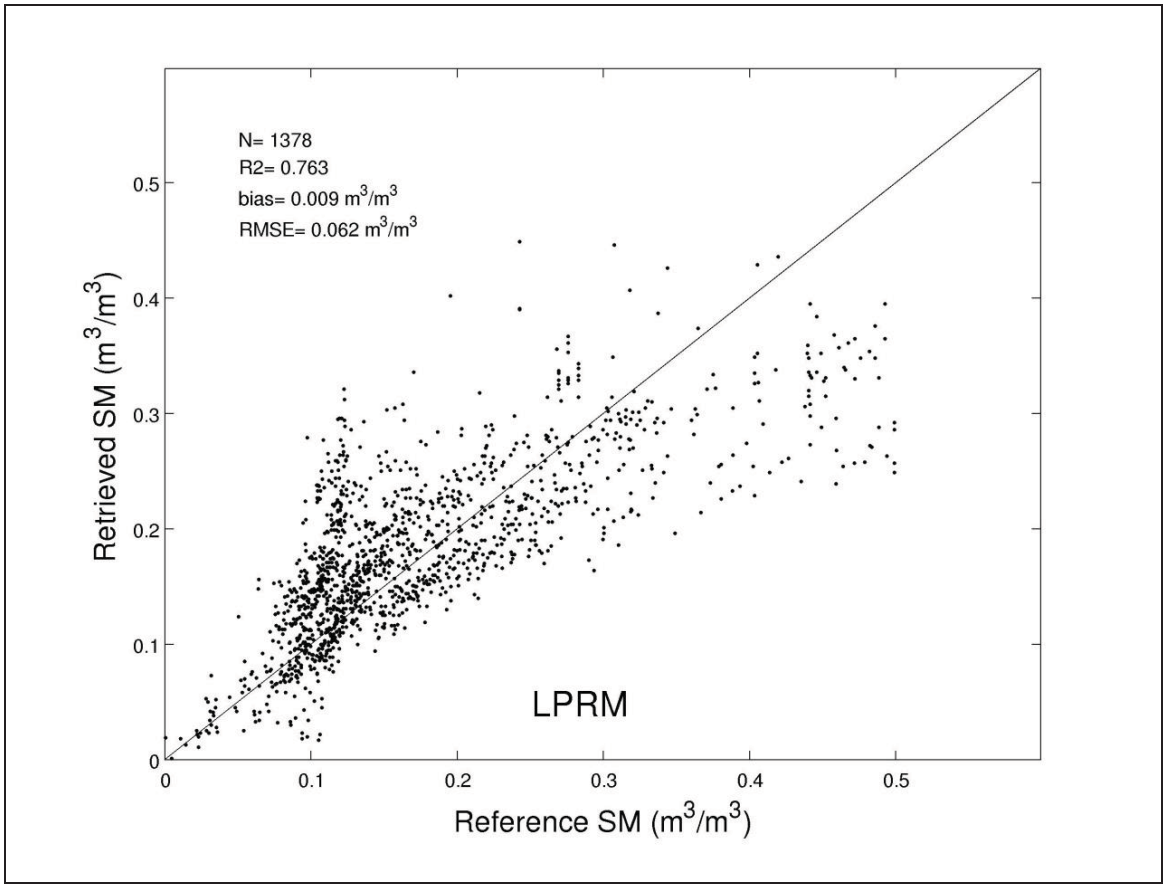
N= 1378
R2= 0.763
bias= 0.009 m3/m3
RMSE= 0.062 m3/m3
LPRM
Retrieved SM (m3/m3)
Reference SM (m3/m3)
0
0.1
0.2
0.3
0.4
0.5

938

939

940 e)

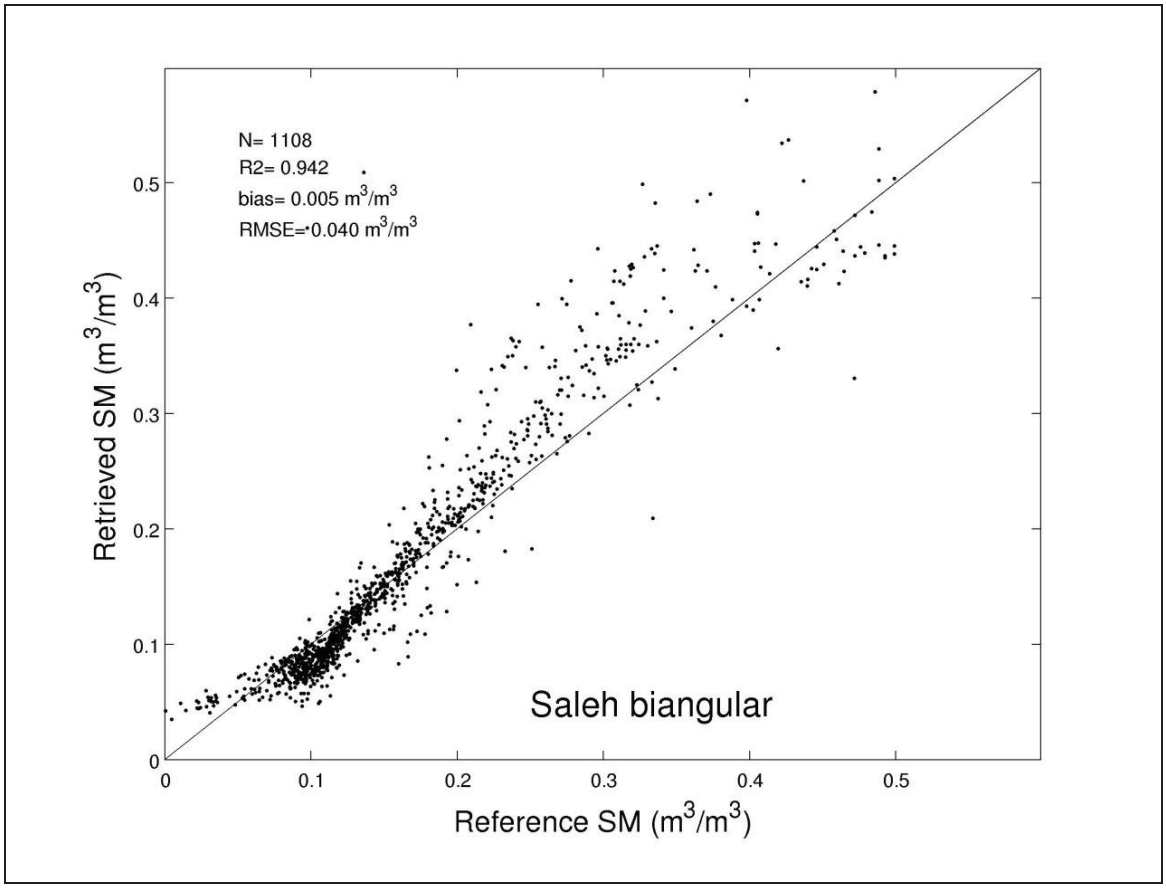
N= 1108
R2= 0.942
bias= 0.005 m3/m3
RMSE= 0.040 m3/m3
Retrieved SM (m3/m3)
Reference SM (m3/m3)
Saleh biangular
0
0.1
0.2
0.3
0.4
0.5

941

942

943 f)

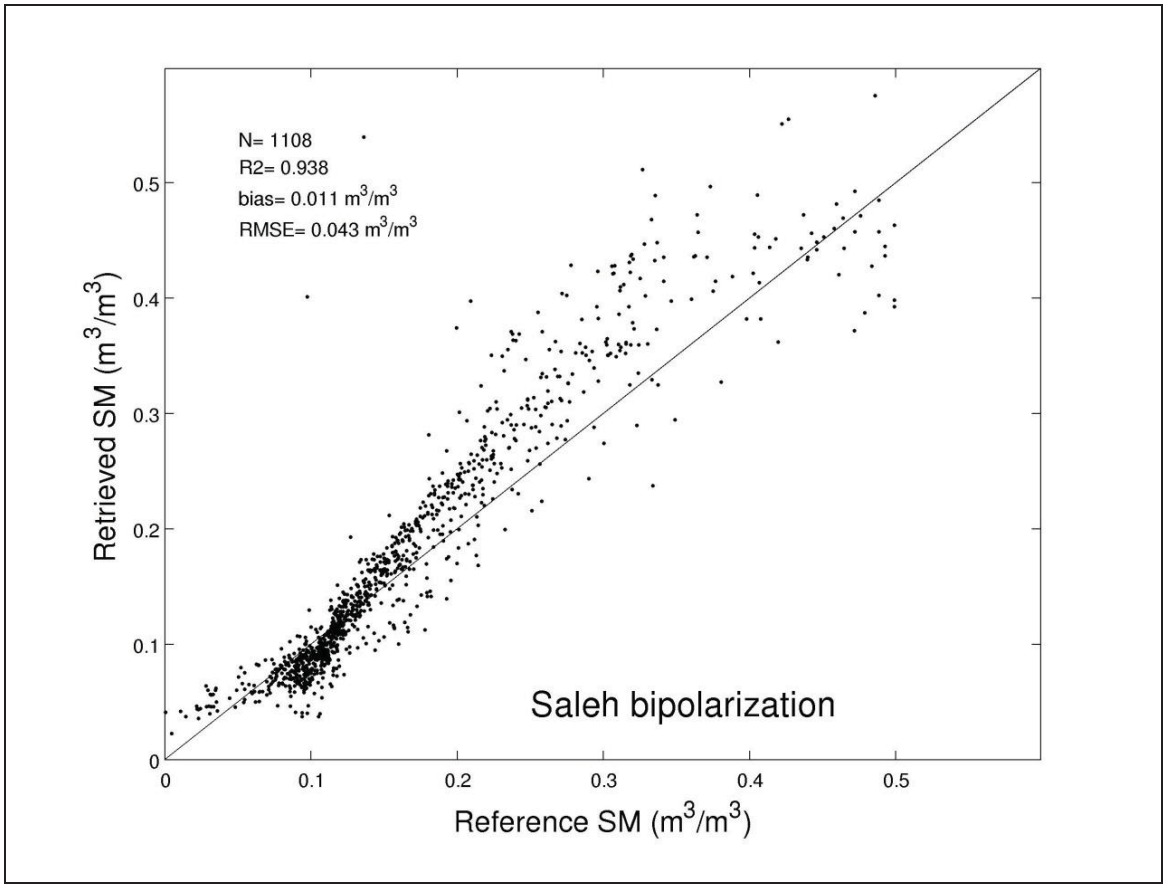
N= 1108
R2= 0.938
bias= 0.011 m3/m3
RMSE= 0.043 m3/m3
Saleh bipolarization
Retrieved SM (m3/m3)
Reference SM (m3/m3)
0
0.1
0.2
0.3
0.4
0.5

944

945

946

947 g)

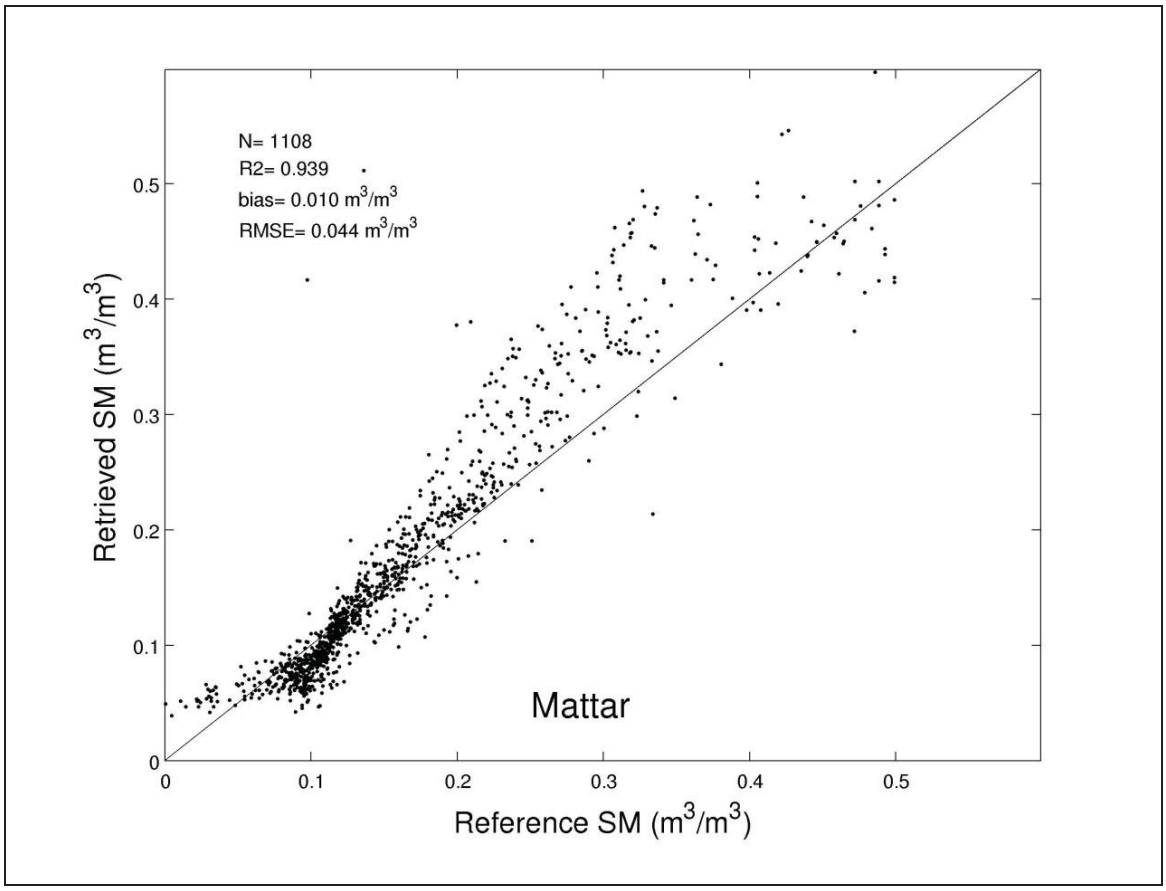

948

949

950